

Tractable Resource Management with Uplink Decoupled Millimeter-Wave Overlay in Ultra-Dense Cellular Networks

Jihong Park, Seong-Lyun Kim, and Jens Zander

Abstract—The forthcoming 5G cellular network is expected to overlay millimeter-wave (mmW) transmissions with the incumbent micro-wave (μ W) architecture. The overall mm- μ W resource management should therefore harmonize with each other. This paper aims at maximizing the overall downlink (DL) rate with a minimum uplink (UL) rate constraint, and concludes: mmW tends to more focus on DL transmissions while μ W has high priority for complementing UL, under time-division duplex (TDD) mmW operations. Such UL dedication of μ W results from the limited use of mmW UL bandwidth due to high peak-to-average power ratio (PAPR) at mobile users. To further relieve this UL bottleneck, we propose mmW UL decoupling that allows a μ W base station (BS) to receive mmW signals. Its impact on mm- μ W resource management is provided in a tractable way by virtue of a novel closed-form mm- μ W spectral efficiency (SE) derivation. In an ultra-dense cellular network (UDN), our derivation verifies mmW (or μ W) SE is a logarithmic function of BS-to-user density ratio. This strikingly simple yet practically valid analysis is enabled by exploiting stochastic geometry in conjunction with real three dimensional (3D) building blockage statistics in Seoul, Korea.

Index Terms—Ultra-dense cellular networks, millimeter-wave, heterogeneous cellular networks, radio resource management, time-division duplex, uplink decoupling, stochastic geometry, 3D blockage model.

I. INTRODUCTION

Spectrum bandwidth increase has been playing a key role to improve data rate in cellular history. The upcoming 5G cellular networks aiming at the 1,000-fold rate improvement, however, can no longer count solely on the existing micro-wave (μ W) spectrum bandwidth. The exploration to resolve this spectrum scarcity has recently reached the use of millimeter-wave (mmW) spectrum whose bandwidth is hundreds times larger than μ W bandwidth [1]–[7]. It leads to the dual radio access technology (RAT) operations in 5G where mmW transmissions are overlaid on top of the legacy μ W cellular architecture [1], [2], [4].

To reach the highest capacities for 5G, interest has lately been turning toward ultra-dense BS deployment [4], [7]–[10]. It is an effective way to enhance μ W cellular capacity in place of bandwidth increase under the μ W spectrum depletion. Besides, this approach fits nicely into mmW transmissions. Deploying more BSs assists in assuring line-of-sight (LOS) conditions for mmW transmissions. This thereby mitigates severe distance attenuation due to physical blockages, which is a major drawback of utilizing mmW spectrum [11]. In this

respect, paving the way for a mm- μ W ultra-dense cellular network (UDN) is of our prime concern.

The critical challenge to such a network operation is the disjunction between downlink (DL) and uplink (UL) rates. It results from employing extremely wide mmW bandwidth. DL rate increase straightforwardly accords with the entire mmW bandwidth. UL users, in contrast, cannot exploit the entire bandwidth despite their exclusive BS access allowed by a minuscule number of UDN per-cell users. The reason follows from low power amplifier efficiency at transmissions [1], [2], captured by high peak-to-average-ratio (PAPR) in this article. It puts a cap on mmW UL bandwidth, leading to significant DL/UL rate discrepancy. This rate mismatch may impinge on user experiences during DL/UL symmetric services such as high-definition video calling. Furthermore, it may hold back improving DL rate when UL rate cannot cope with the required control signals for DL.

In view of tackling this bottleneck, we focus on mm- μ W DL/UL resource management, and jointly adjust their allocations so as to maximize the overall mm- μ W DL rate while guaranteeing a minimum UL/DL rate ratio. For given mm- μ W bandwidths, this paper answers the question: *how much portion of mm- μ W resources should be allocated to UL transmissions as mmW BS deployment proliferates.*

The solution of such resource management hinges on the mm- μ W spectral efficiency (SE) calculation. In this paper, we derive the closed-form SEs in a mm- μ W UDN by using stochastic geometry. In addition to its providing tractability in mm- μ W resource management, the closed-form result reveals the following UDN characteristics: (i) UDN SE is a *logarithmic function of BS-to-user density ratio*; and (ii) a UDN is *weak interference-limited* where its behaviors toward BS densification and blockages are analogous to the trends in a noise-limited regime.

Motivated by the fact UDN SE increases along with BS densification, we propose a novel *mmW UL decoupling* technique that further alleviates the UL rate bottleneck. It allows μ W BSs to receive mmW UL signals, yielding the impact on a par with UL mmW BS densification. The corresponding mm- μ W UDN resource management and overall DL rate are numerically validated under a three dimensional (3D) mmW blockage model combined with the actual building statistics in Seoul, Korea.

A. Related Works

Utilizing mmW spectrum in 5G cellular networks has recently been viewed as of paramount importance in both industry [1], [3], [4] and academia [5]–[7], [12], [13]. Its point-to-point-wise cellular network applicability was validated by

J. Park and S.-L. Kim are with School of Electrical & Electronic Engineering, Yonsei University, Seoul, Korea (email: jhpark.james@yonsei.ac.kr, slkim@yonsei.ac.kr).

J. Zander is with Wireless@KTH, KTH – The Royal Institute of Technology, Stockholm, Sweden (email: jenz@kth.se).

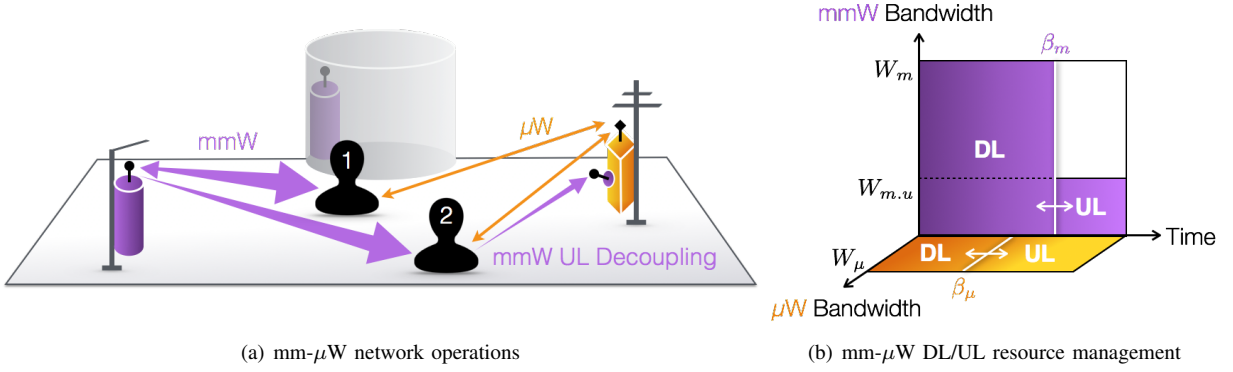


Fig. 1. Illustrations of mm- μ W network operations and its DL/UL resource management under mmW non-penetrable building blockages: **Associations.** Each user has a pair of dual connections for mm- μ W receptions/transmissions based on the strongest received power association rule. By the aid of *mmW UL decoupling*, mmW UL users are also able to associate with μ W BSs if they provide stronger UL signals than mmW BSs (compare user 2 with user 1); **DL/UL Rate Asymmetry.** mmW UL bandwidth is limited by PAPR at mobiles (see $W_{m,u} < W_m$), and thus its corresponding UL rate is smaller than DL rate; **DL/UL Allocations.** Given TDD operations, mm- μ W UL allocation ratios are determined via adjusting β_m and β_μ .

indoor/outdoor channel modeling [5], [6] as well as by laboratory demonstration [3]. For its network-wide deployment, the authors [12], [13] analyzed the mmW indoor/outdoor cellular network from the coverage probability and average rate perspectives. On the basis of these preceding efforts, this study considers both mmW and the incumbent μ W coexisting heterogeneous networks that are highly promising phased deployment scenarios toward 5G [4], [7]. Starting from this dual-RAT structure, we focus on a higher layer design guideline how to jointly manage the mm- μ W radio resources for DL/UL transmissions.

When it comes to the UDN impact, previous investigations paid attention to its complementing the blockage-vulnerable drawback of mmW [11] and reducing interference [14]–[20]. The decrease in UDN interference follows from the turned-off BSs having no serving users according to the Third Generation Partnership Project (3GPP) Release 12 specifications [21]. This article embodies both ultra-densification effects on SE improvement, and provides closed-form mm- μ W UDN SEs.

Note that our preliminary research about mm- μ W UDN [18], [19] in part includes similar arguments to this article but under different scenarios. Specifically, an indoor/outdoor modeling is considered in [18], and a 3D blockage model with actual building geography is incorporated in [19]. Both works are based on frequency-division duplex (FDD) mmW operations unlike the time-division duplex (TDD) mmW operations in this article. From an analytic perspective, the closed-form μ W UDN SE derivation was first introduced in [17] with its economic impact, based on a lower bound approximation. This article provides the upper bound for completeness, and also derives mmW UDN SE extending the analytic applicability.

In addition, it is worth mentioning that this study is on the basis of our UDN definition where the number of BSs exceeds the number of users (see Definition 1) as in [17]–[20], [22], [23]. Therefore, the UDN SE arguments in this article may not be in line with other opinions, especially regarding the near-field effect that may degrade SE under a scenario neglecting the turned-off BS impact [24], [25]. Incorporating the near-field effect with our UDN definition is deferred to the partially loaded scenario in [23].

B. Contributions and Organizations

The main contributions of this paper are listed as follows.

- *Closed-form mm- μ W UDN SEs* are derived, enabling tractable mm- μ W resource management. The representations of both DL/UL mmW (or μ W) UDN SEs are identically a logarithmic function of the BS density normalized by user density (Theorems 1 and 2 in Section III-A).
- The mm- μ W UL resource allocation strategy is provided in order to maximize DL rate with a minimum UL/DL rate ratio constraint as follows: along with the mmW BS densification, *μ W UL allocation increases, and mmW UL allocation grows only after using up the entire μ W bandwidth.* This in the end leads to the *UL dedicated μ W spectrum* that contradicts with the traditional μ W cellular resource management trend (Propositions 3 and 4 in Section IV-C).
- To further rein back DL/UL rate asymmetry, *mmW UL decoupling* is proposed. The technique allows μ W BSs to receive mmW UL signals. This thereby increases mmW UL rate, resulting in up to 1.64 times overall DL rate improvement in given scenarios (Propositions 5 and 6 in Section IV-D).
- The mm- μ W DL/UL resource allocations are numerically estimated on the basis of a *realistic 3D building blockage model*. The calculation incorporates the actual building locations, sizes, and heights in Seoul, Korea (Table I in Section V-A).

The rest of the paper is organized as follows. The mm- μ W network environment and its operations are specified in Section II. The closed-form mm- μ W UDN SEs are derived in Section III. The results are utilized for providing tractable mm- μ W resource management as well as for emphasizing the mmW UL decoupling impact in Section IV. Numerical evaluation under a real data based 3D building blockage model is presented in Section V followed by concluding remarks in Section VI. The proofs of lemmas and propositions are provided respectively in Appendices I and II.

II. SYSTEM MODEL

A. Millimeter-Wave Overlaid Cellular Network

A mm- μ W network consists of mmW and μ W BSs. The locations of mmW BSs follow two-dimensional (2D) homogeneous Poisson point process (PPP) Φ_m with density λ_m [26]. Similarly, the μ W BS coordinates follow a homogeneous PPP Φ_μ with density λ_μ , independent of Φ_m . Mobile user coordinates independently follow a homogeneous PPP Φ_u with density λ_u . Without loss of generality, Φ_u denotes either DL or UL users with the same density. For simplicity, we hereafter only focus on outdoor users whose coordinates do not overlap with building blockages. The blockage modeling is specified in Section II-B.

As Fig. 1 visualizes, users simultaneously associate with mmW and μ W BSs via different antennas for each as in macro-and-small-cell dual connectivity [27]. The associations of users for both mmW and μ W are based on the maximum received signal powers. Control signals are communicated via μ W so as to guarantee the connections regardless of blockages. The control signal traffic is assumed to be negligible when calculating data rates since the volume is much less than that of data transmissions.

Regarding multiple associations of users at a BS, the BS selects a single active user per unit time slot according to a uniformly random scheduler. The selected active users are denoted as $\Phi_{\hat{u}}$. The mmW (or μ W) BSs having at least a single active user are represented by $\Phi_{\hat{m}}$ (or $\Phi_{\hat{\mu}}$). Note that $\Phi_{\hat{u}}$, $\Phi_{\hat{m}}$, and $\Phi_{\hat{\mu}}$ are non-homogeneous PPPs due to their location dependent active user selections; for instance, a user having more neighboring BSs (or smaller Voronoi cell size of the associated BS) is selected with higher probability, incurring location dependency. The mm- μ W BSs having no associated users are turned-off.

B. Blockage Model

Consider building blockages that cannot be penetrated by mmW signals. Every single mmW signal reception should therefore ensure the line-of-sight (LOS) condition between its transmitter-receiver pair. According to the average LOS model [12], assume that LOS is guaranteed when a given transmitter-receiver distance r is within an LOS distance R_L that is determined by the site geography of a network. The LOS indicator function $\mathbb{1}_{R_L}(r)$ represents such a model, which returns unity if LOS exists, i.e. $r \leq R_L$; otherwise zero.

The value of R_L with the 2D blockage model [12], [13], [28], [29] is directly computed by utilizing building perimeters, areas, and coverage from actual geographical data. For the 3D blockage model, the calculation of R_L additionally incorporates building heights, to be further elaborated in Section V-A. Throughout this paper, we by default consider the 3D blockage model, but apply a 2D channel model that provides more tractability. Incorporating a 3D channel model with the 3D blockage model is deferred to future work. In contrast to mmW signals, μ W signals are not affected by blockages thanks to their high diffraction and penetration characteristics.

C. Channel Model

A mmW antenna array at a BS (or user for UL) directionally transmits a signal with power $P_{m.d}$ (or $P_{m.u}$) in units of watt to its associated user (or BS). For simplicity, the antenna array gains at mmW transmitters and receivers are assumed to be unity. The transmitted mmW signal experiences path loss attenuation with the exponent $\alpha_m > 2$ as well as Rayleigh fading with unity mean, i.e. channel fading power $g \sim \exp(1)$. Note that LOS dependent mmW scenarios may be more in line with Rician fading, which incorporates the number of LOS paths, or Nakagami- m fading that can be a mean value approximation of the Rician fading by adjusting its shape factor m . The Rayleigh model in this paper nevertheless enables better tractability while providing at least a lower bound of the maximized DL rate under Nakagami- m fading. That is because the signal-to-interference-plus-noise (SINR) with Nakagami- m fading is lower bounded by the value with Rayleigh fading, verified via a stochastic ordering technique [30].

The transmitted directional mmW signal has a main lobe beam width θ radian, and its beam center $\Theta \in [0, 2\pi]$ pointing at the associated user (or BS). The received signal powers at the same distances within the mainlobe are assumed to be identical, and sidelobes are neglected for simplicity. Accordingly, at a receiver, interferers are the transmitters whose main lobes cover the location of the receiver. When interference is treated as noise, by the aid of Slyvnyak's theorem [26], DL/UL mmW SINR at a typical user (or BS) is represented as:

$$\text{SINR}_{m.d} := \frac{P_{m.d} g r^{-\alpha_m} \mathbb{1}_{R_L}(r)}{\sum_{i \in \Phi_{\hat{m}}} \Theta_i P_{m.d} g_i r_i^{-\alpha_m} \mathbb{1}_{R_L}(r_i) + \sigma^2} \quad (1)$$

$$\text{SINR}_{m.u} := \frac{P_{m.u} g r^{-\alpha_m} \mathbb{1}_{R_L}(r)}{\sum_{i \in \Phi_{\hat{u}}} \Theta_i P_{m.u} g_i r_i^{-\alpha_m} \mathbb{1}_{R_L}(r_i) + \sigma^2} \quad (2)$$

where r and r_i respectively denote the distances to the associated BS (or user) and interfering BSs (or users) from the origin, σ^2 noise power, and Θ_i the probability that the i -th transmitter interfering with the typical receiver. Note that Θ_i is a uniformly random variable since the associated receiver location of the i -th interfering transmitter is also uniformly distributed.

The μ W channel model is similar to the mmW model. The only differences are its omnidirectionally transmitted signal with power $P_{\mu.d}$ (or $P_{\mu.u}$) under path loss exponent $\alpha_\mu > 2$ and neglecting blockage effect. At a typical user (or BS), the μ W SINR is then given as:

$$\text{SINR}_{\mu.d} := \frac{P_{\mu.d} g r^{-\alpha_\mu}}{\sum_{i \in \Phi_{\hat{\mu}}(\text{or } \Phi_{\hat{u}})} P_{\mu.d} g_i r_i^{-\alpha_\mu} + \sigma^2} \quad (3)$$

$$\text{SINR}_{\mu.u} := \frac{P_{\mu.u} g r^{-\alpha_\mu}}{\sum_{i \in \Phi_{\hat{u}}(\text{or } \Phi_{\hat{\mu}})} P_{\mu.u} g_i r_i^{-\alpha_\mu} + \sigma^2}. \quad (4)$$

Now that our interest of this paper is confined to ultra-dense cellular networks, we hereafter only consider signal-to-interference-ratio (SIR) instead of SINR by neglecting σ^2 under a interference-limited regime.

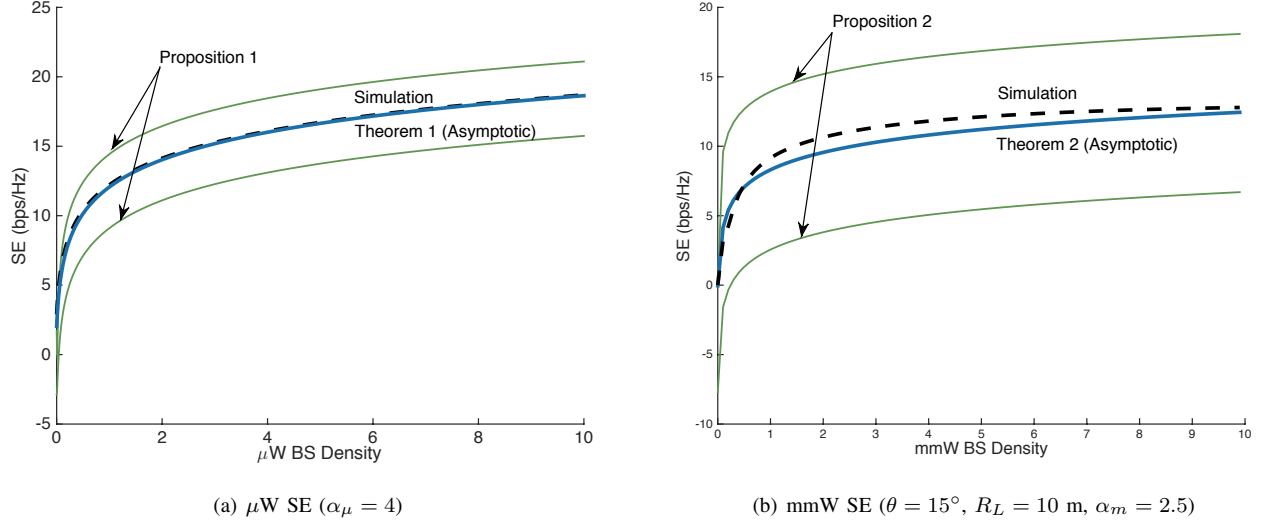


Fig. 2. The mm- μ W DL/UL UDN SE upper and lower bounds as well as asymptotic values when $\lambda_u = 0.01$.

D. Resource Management under Limited mmW UL Spectrum

Consider multiple access of mm- μ W users follows orthogonal frequency-division multiple access (OFDMA) during each unit time slot. The entire mm- μ W spectrum bandwidths are given respectively as W_m and W_μ .

For mmW, DL/UL resources are allocated in a time-division duplex (TDD) manner via adjusting the mmW UL allocation ratio β_m . While mmW DL operates with the entire W_m , mmW UL operations only utilize $W_{m,u} < W_m$ due to the PAPR outage at mobile users in return for the use of huge W_m (see Fig. 1). Specific mmW UL PAPR outage constraint is deferred to Section IV.

Note that the said mmW UL PAPR bottleneck can be relaxed via single-carrier frequency-division multiple access (SC-FDMA). Increasing $W_{m,u}$ close to W_m in such a scenario, however, still brings about another bottleneck. For instance, the sampling rate of analog-to-digital converter (ADC) should be at least $2W_{m,u}$ according to Nyquist-Shannon theorem. This huge sampling rate becomes an UL bottleneck by linearly increasing ADC power consumption at mobile users [31], incorporated in future work.

For μ W, DL/UL resource allocation follows TDD via adjusting μ W UL allocation ratio β_μ . This model is also able to capture FDD based μ W operations whose UL spectrum allocation is $\beta_\mu W_\mu$. In any cases, μ W bandwidth W_μ is much smaller than W_m , and therefore μ W UL operations are assumed to be free from the PAPR outage at mobile users.

III. SPECTRAL EFFICIENCIES OF MILLIMETER-WAVE OVERLAID ULTRA-DENSE CELLULAR NETWORKS

The closed-form representations for mm- μ W SEs are of prime concerns in this section. The derived results will play a salient role in tractable mm- μ W resource management in Section IV. The SE is defined as ergodic capacity $E \log[1 + \text{SINR}]$, in units of nats/sec/Hz (1bit ≈ 0.693 nats) unless otherwise noted. Unlike μ W SE, mmW SE incorporates the degradation resulting from blockages. Its impact is captured via average

LOS distance R_L . We hereafter let the subscripts m and μ denote mmW and μ W respectively. The path loss exponent α and BS density λ without subscripts can be either mmW or μ W, which improves notational reusability. In the following subsections, closed-form mm- μ W SEs are first presented in Section III-A, and then their derivations are described in the remainder of the subsections.

A. Closed-form mm- μ W UDN SEs

For a BS density λ , let $\hat{\lambda}$ denote λ/λ_u . This ratio of BS-to-user density determines the ultra-densification of a network as follows.

Definition 1. (UDN) *A cellular network with BS density λ is called a UDN where $\hat{\lambda} \gg 1$. The notation $f \gg g$ implies f is sufficiently large so that $O(g/f)$ is approximated by 0.*

In a UDN regime, the difference between DL and UL μ W SEs, denoted respectively by $\gamma_{\mu,d}$ and $\gamma_{\mu,u}$, is negligible. That is because most of the associated user-BS distances of both DL and UL become identical. Such a UDN regime, furthermore, leads to the asymptotic convergence of the upper and lower bounds of $\gamma_{\mu,d}$ (or $\gamma_{\mu,u}$) as $\hat{\lambda}_\mu$ increases. Its derivation is deferred to Proposition 1 in Section III-C. The corresponding asymptotic μ W UDN SE is presented in the theorem below.

Theorem 1. (Asymptotic μ W UDN SE) *For $\hat{\lambda}_\mu \rightarrow \infty$, DL and UL μ W SEs identically converge to γ_μ , i.e. $\gamma_\mu = \lim_{\hat{\lambda}_\mu \rightarrow \infty} \gamma_{\mu,u} = \lim_{\hat{\lambda}_\mu \rightarrow \infty} \gamma_{\mu,d}$, and the value is given as:*

$$\gamma_\mu = \frac{\alpha_\mu}{2} \log \hat{\lambda}_\mu. \quad (5)$$

In a similar manner, mmW DL and UL SEs are denoted respectively by $\gamma_{m,d}$ and $\gamma_{m,u}$, and their values become identical in a UDN regime. The upper and lower bounds of $\gamma_{m,d}$ (or $\gamma_{m,u}$) converge as specified at Proposition 3 in Section III-D. The converged mmW UDN SE is stated in the following theorem.

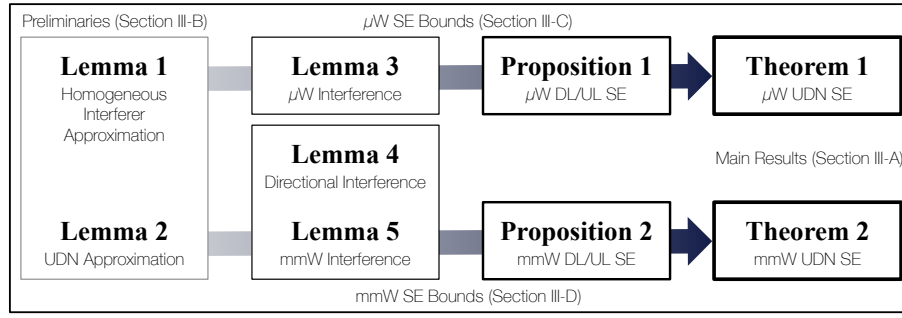


Fig. 3. Mathematical technique connections toward the derivations of Theorems 1 and 2.

Theorem 2. (Asymptotic mmW UDN SE) For $\hat{\lambda}_m \rightarrow \infty$, DL and UL mmW SEs identically converge to γ_m , i.e. $\gamma_m = \lim_{\hat{\lambda}_m \rightarrow \infty} \gamma_{m,u} = \lim_{\hat{\lambda}_m \rightarrow \infty} \gamma_{m,d}$, and the value is given as:

$$\gamma_m = \frac{\alpha_m p_L}{2} \log \hat{\lambda}_m \quad (6)$$

where $p_L := 1 - \exp(-\lambda_m \pi R_L^2)$.

The results are illustrated in Fig. 2. According to Theorems 1 and 2, both mm- μ W SEs have two remarkable characteristics under a UDN regime as follows.

Remark 1. (BS-to-User Density Ratio Dependence) UDN SE logarithmically increases with BS-to-user density ratio.

This first finding emphasizes what matters in a UDN is the ratio of BS density to user density, also highlighted via simulation in [20]. In addition, it is worth noticing that the result above is distinct from the well-known SE behavior that is independent of BS densification under an interference-limited regime [32]. Such a difference is caused by unique characteristics of UDN interference that is limited by user density. In a DL UDN, for instance, user density puts a cap on interference increase since it determines whether a BS becomes an interferer via turning on/off the BS. On the other hand, BS densification increases the desired signal power via reducing the association distance by $1/(2\sqrt{\lambda})$ on average, resulting in the logarithmic SE improvement.

The second finding includes the exposition of a new-found *weak-interference regime* that has a mixed nature of interference/noise-limited behaviors as follows.

Remark 2. (Weak Interference-Limited UDN) An interference-limited UDN shows distinctive behavior toward mmW blockages and BS densification, which is similar to the trends in a noise-limited regime.

Clear understanding of this unique UDN trait follows from revisiting an interference-limited network whose noise power is negligible compared to interference, i.e. $\text{SINR} \approx \text{SIR}$. In a traditional interference-limited network, it is well known that SE increases along with path loss exponent [32] and blockages [12]. Their corresponding interference reductions dominate the desired power decreases, thereby leading to SE increases. Under this interference-limited network, in addition, SE is independent of BS densification and transmission power increase [32]. The reason is they improve the desired signal

power and interference alike, thus cancelling their impact each other.

In an interference-limited UDN, the effects of path loss exponent and transmission power increase directly follow the same trends in a traditional interference-limited network. On the other hand, the increase in blockages, i.e. increasing p_L via reducing R_L , decreases mmW UDN SE. That is because a large number of mmW UDN interferers dominate the blocked interferers. It makes the interference reduction due to blockages negligible. The UDN SE therefore depends solely on the desired signal power decrease due to blockages. Unlike a traditional interference-limited network, it is also remarkable that BS densification increases UDN SE in a logarithmic manner as stated after Remark 1. Such trends toward blockages and BS densification under an interference-limited UDN are analogous to the behaviors in a traditional noise-limited network where interference is negligible compared to noise.

When reminding of the UDN interference delimited by user density, it is worth mentioning that a UDN with low user density may become noise-limited. Nevertheless, its trivial tendency due to removing interfering interaction is not of our interest, thus neglected. The following subsections describe the major techniques for the derivations of Theorems 1 and 2. The relationship of the techniques are summarized in Fig. 3.

B. Preliminary Techniques

This section introduces two approximations that are feasible under a UDN regime. These techniques make a detour around the obstacles disrupting the tractable SE analysis.

The first technique tackles the nonhomogeneity of the interferers, active BSs for DL and active users for UL. As described in Section II-A, this intractability is induced by the random active user selection at multiple access. The selection probability of active users depends on each BS's cell coverage whose size is affected by its neighboring BSs; for instance, a user in a BS dense region is more likely to be selected due to the small cell coverage size of the associated BS. This inter-node dependency results in non-homogeneous interferer distributions.

In a UDN regime, however, such a location dependency diminishes since cell size tends to be identical. We thus approximate the interferers are independently thinned. The thinning probability for DL is active BS probability p_a , and for

$$\log \left(1 + \left[\rho_\mu^{-1} \hat{\lambda}_\mu \right]^{\frac{\alpha_\mu}{2}} \right) - \frac{\alpha_\mu}{2} \leq \gamma_{\mu,d} \text{ (or } \gamma_{\mu,u}) \leq \log \left(1 + \left[\left(1 + \frac{2}{\alpha_\mu} \right) \hat{\lambda}_\mu \right]^{\frac{\alpha_\mu}{2}} \right) - \frac{\alpha_\mu}{2} \quad (12)$$

UL is user selection probability p_s , derived in [14] as follows.

$$p_a = 1 - \left[1 + (3.5\hat{\lambda})^{-1} \right]^{-3.5} \quad (13)$$

$$p_s = p_a \hat{\lambda} \quad (14)$$

The corresponding interferer distribution is specified in the following lemma.

Lemma 1. (Homogeneous Interferer Approximation) *As $\hat{\lambda} \rightarrow \infty$, both DL and UL interferer coordinates identically converge to a homogeneous PPP with density λ_u .*

This underpins the homogeneous PPP approximation of the interferer coordinates in a UDN regime, of which the validity is also investigated by simulation in [15]. The result intuitively implies that the interferer coordinates converge to user coordinates in a UDN regime. It is therefore important to note that such a homogeneous PPP approximation is valid only when users are uniformly distributed. This emphasizes the impact of user distribution in a UDN regime, to be incorporated in future work.

The second technique enhances the tractability of the SE representations. As an example of the SE calculation, consider a DL UDN with BS density λ . At a typical user, the associated BS is the nearest BS out of the entire BSs deployed with density λ while the interferers are active BSs whose density is approximated as λ_u (or $p_a \lambda$) via Lemma 1. Exploiting Campbell theorem [26] with the same technique at the equation (16) in [32], the corresponding DL UDN SE γ_d is represented as

$$\gamma_d = \int_{t>0} \mathbb{E}_R \left[\exp \left(-\lambda_u \pi (e^t - 1)^{\frac{2}{\alpha}} r^2 \int_{(e^t-1)^{-\frac{2}{\alpha}}}^{\infty} \frac{du}{1+u^{\frac{\alpha}{2}}} \right) \right] dt \quad (9)$$

where R denotes the distance to the associated BS from the typical user.

Nevertheless, this representation is not tractable due to the innermost integration range that depends on t . To remove such a dependency, we first exploit the following approximation proposed in our preliminary work [17], which is tight in a UDN regime.

Lemma 2. (UDN Approximation) *Consider a UDN with BS density λ . For a nonnegative constant $I \ll \lambda$, the following approximation holds.*

$$\mathbb{E}_R [\exp(-\lambda_u \pi r^2 I)] \approx [1 - \hat{\lambda}^{-1} I]^+ \quad (10)$$

In the following Sections III-C and D, this result will be combined with (9), and leads to tractable upper and lower bounds of μ W and mmW DL/UL SEs, each of which identically converges on the asymptotic closed-form SE respectively in Theorems 1 and 2.

C. μ W SE Bounds (Derivation of Theorem 1)

Let $\rho_\mu^{(t)}$ denote μ W interference constant defined as $\int_{(e^t-1)^{-\frac{2}{\alpha_\mu}}}^{\infty} \frac{du}{1+u^{\frac{\alpha_\mu}{2}}}$. This corresponds with the innermost integration in (9). To avoid double integration in (9) for tractability, we consider the lower and upper bound of $\rho_\mu^{(t)}$ as below.

Lemma 3. (μ W Interference Constant Bounds) *The following inequality holds for all $t > 0$*

$$\left(1 + \frac{2}{\alpha_\mu} \right)^{-1} - (e^t - 1)^{-\frac{2}{\alpha_\mu}} \leq \rho_\mu^{(t)} \leq \rho_\mu \quad (11)$$

where $\rho_\mu := \int_{u>0} \frac{du}{1+u^{\frac{\alpha_\mu}{2}}} = \left(\frac{2\pi}{\alpha_\mu} \right) \csc \left(\frac{2\pi}{\alpha_\mu} \right)$.

Applying Lemmas 2 and 3 to (9) provides the following tractable upper and lower bounds of μ W DL/UL UDN SEs.

Proposition 1. (μ W DL/UL UDN SE Bounds) *In a UDN regime, μ W DL SE $\gamma_{\mu,d}$ and UL SE are identically bounded as (12) at the top of the page.*

This result reveals that μ W DL/UL SEs share the same upper and lower bounds in a UDN regime. The reason is because the user-to-interfering active BS distances asymptotically converge on the inter-user distances as BS density increases.

In addition, the proposition shows the upper and lower bounds of μ W DL/UL UDN SEs logarithmically increases with the BS-to-user density ratio. For the DL, the improvement in SE results from the fact that BS densification reduces its corresponding Voronoi cell sizes. This turns off the BSs having no active user within their cells. Consequently, at a typical user, the interfering active BSs decrease, and their density ends up with being delimited by user density (recall Lemma 1). At the same time, the densification shortens the distance between a typical user and its associated BS, thereby yielding the SE increase.

For the UL, the SE improvement follows from the cell size reduction along with densification in a similar way to the DL case. The difference is the BS densification may increase interferers by increasing the number of the selected users. In a UDN regime, nevertheless, such an interferer increasing effect rarely occurs, leading to improve the SE as in the DL scenario.

D. mmW SE Bounds (Derivation of Theorem 2)

Directional mmW signal transmissions decrease the aggregate interference at a typical receiver compared to omnidirectional transmissions. The reduced interference amount is specified as below.

Lemma 4. (Directional Interference Thinning) *At a typical user (or BS), DL mmW aggregate interference $I_{\Sigma_{m,d}}$ and UL*

$$\int_{t>0} p_L^{(t)} \left(1 - \rho_m \hat{\lambda}_m^{-1} \left[\frac{\theta}{2\pi} (e^t - 1) \right]^{\frac{2}{\alpha_m}} \right)^+ dt \leq \gamma_{m,d} \text{ (or } \gamma_{m,u}) \leq \int_{t>0} p_L^{(t)} \left(1 - \left[\left(1 + \frac{2}{\alpha_m} \right) \hat{\lambda}_m \right]^{-1} \left[\frac{\theta}{2\pi} (e^t - 1) \right]^{\frac{2}{\alpha_m}} \right)^+ dt \quad (16)$$

$$p_L \left[\log \left(1 + \frac{2\pi}{\theta} \left[\rho_m^{-1} \hat{\lambda}_m \right]^{\frac{\alpha_m}{2}} \right) - \frac{\alpha_m}{2} \right] \leq \gamma_{m,d} \text{ (or } \gamma_{m,u}) \leq C_{L_2} \log \left(1 + \frac{2\pi}{\theta} \left[\left(1 + \frac{2}{\alpha_m} \right) \hat{\lambda}_m \right]^{\frac{\alpha_m}{2}} \right) \quad (17)$$

where $p_L^{(t)} := 1 - e^{-\lambda_m \pi R_L^2 \left\{ 1 + \hat{\lambda}_m^{-1} \rho_m \left[\frac{\theta}{2\pi} (e^t - 1) \right]^{\frac{2}{\alpha_m}} \right\}}$ and $C_{L_2} := 1 - e^{-\lambda_m \pi R_L^2 \left\{ 1 + \rho_m \left(1 + \frac{2}{\alpha_m} \right) \right\}}$

mmW aggregate interference $I_{\Sigma_{m,u}}$ are represented as:

$$I_{\Sigma_{m,d}} \approx \sum_{i \in \Phi_m \left(\lambda_u \left(\frac{\theta}{2\pi} \right)^{\frac{2}{\alpha_m}} \right)} g_i r_i^{-\alpha_m} \mathbb{1}_{R_L}(r_i) \quad (13)$$

$$I_{\Sigma_{m,u}} \approx \sum_{i \in \Phi_u \left(\lambda_u \left(\frac{\theta}{2\pi} \right)^{\frac{2}{\alpha_m}} \right)} g_i r_i^{-\alpha_m} \mathbb{1}_{R_L}(r_i). \quad (14)$$

The rest of the derivation follows the similar procedure for the μ W case in Section III-C. Let $\rho_m^{(t)} := \int_{(e^t-1)^{-\frac{2}{\alpha_m}}}^{\left(\frac{R_L}{r}\right)^2 (e^t-1)^{-\frac{2}{\alpha_m}}} \frac{du}{1+u} \frac{du}{\frac{\alpha_m}{2}}$. The following lemma provides tractable upper and lower bounds of $\rho_m^{(t)}$.

Lemma 5. (mmW Interference Constant Bounds) *The following inequality holds: (i) for $\hat{\lambda}_m \rightarrow \infty$ almost surely; and (ii) for a UDN with probability $1 - \exp(-\rho_m \lambda_u \pi R_L^2)$.*

$$1 - \left(1 + \frac{\alpha_m}{2} \right)^{-1} - (e^t - 1)^{-\frac{2}{\alpha_m}} \leq \rho_m^{(t)} \leq \rho_m \quad (15)$$

where $\rho_m := \int_{u>0} \frac{du}{1+u} \frac{du}{\frac{\alpha_m}{2}} = \left(\frac{2\pi}{\alpha_m} \right) \csc \left(\frac{2\pi}{\alpha_m} \right)$

In a UDN, it is highly feasible to apply the inequality above for LOS distance and/or user density. According to Table I, our target geography corresponds with such an environment. At Gangnam, for instance, the inequality holds with probability greater than 0.93 ($\lambda_u = 1 \times 10^{-4}$, $\alpha_m = 2.5$). We thus assume Lemma 5 always holds in a UDN hereafter.

The mmW DL/UL UDN SEs are then upper and lower bounded by applying Lemmas 4 and 5 to (9).

Proposition 2. (mmW DL/UL UDN SE Bounds) *In a UDN regime, mmW DL SE $\gamma_{m,d}$ and UL SE $\gamma_{m,u}$ are identically bounded as (16) at the top of this page.*

It shows both DL/UL mmW SEs have the same upper and lower bounds as in the case of μ W SE in Proposition 1. The impact of ultra-densification however cannot be explicitly interpreted in this form due to the integrations therein.

To capture the mmW UDN behavior in a more intuitive way, we consider less tight but more tractable upper and lower bounds. The modified lower bound follows from $p_L \leq p_L^{(t)}$. For the upper bound, observe that the maximum t is $\log \left(1 + \frac{2\pi}{\theta} \left[\left(1 + \frac{2}{\alpha_m} \right) \hat{\lambda}_m \right]^{\frac{\alpha_m}{2}} \right)$ such that the upper bound integrand is non-zero. Combining them provides the following closed-form upper and lower bounds.

Corollary 1. (Tractable mmW DL/UL UDN SE Upper Bound) *In a UDN regime, mmW DL SE $\gamma_{m,d}$ and UL SE $\gamma_{m,u}$ are identically upper bounded as (17) at the top.*

This indicates mmW SE also logarithmically increases with the BS-to-user density ratio as in the μ W SE in Section III-C. The only difference is its average LOS probability p_L due to the blockage vulnerability of mmW signals.

IV. UPLINK/DOWNLINK RESOURCE MANAGEMENT IN MILLIMETER-WAVE UPLINK DECOUPLED ULTRA-DENSE CELLULAR NETWORKS

This section jointly optimizes mm- μ W DL/UL resource allocations so that the overall average DL rate is maximized while guaranteeing a minimum UL rate. In addition, we propose a mmW UL decoupling that further enhances the DL rate without procuring additional spectrum resources. For the calculations including mm- μ W SEs, we henceforth approximate the exact values by the results in Theorems 1 and 2, of which the tightness is validated in Fig. 2.

A. PAPR-limited mmW UL Bandwidth

The mm- μ W resource management incorporates the limited mmW UL spectrum amount $W_{m,u}$ as discussed in Section II-D. Such a problem follows from the PAPR outage constraint at mobile users: $\Pr(\text{PAPR}_u > \delta) \leq \epsilon$ for constants $\delta, \epsilon > 0$ where PAPR_u denotes the PAPR at mobile users. According to [33], the PAPR outage probability is given as

$$\Pr(\text{PAPR}_u > \delta) \approx 1 - \exp \left(-\frac{w e^{-\delta}}{f_s} \sqrt{\frac{\pi \delta}{3}} \right) \quad (18)$$

where w denotes UL spectrum bandwidth and f_s subcarrier spacing. This enables calculating $W_{m,u}$ that corresponds with the maximum w when the PAPR outage probability in (18) meets ϵ as follows.

$$W_{m,u} = \sqrt{3} f_s e^{\delta} (\pi \delta)^{-\frac{1}{2}} (\log \epsilon^{-1})^{-1} \quad (19)$$

B. Problem Formulation

Define DL and UL average rates \mathcal{R}_u and \mathcal{R}_d as follows.

$$\mathcal{R}_u := \beta_m W_{m,u} \gamma_{m,u} + \beta_\mu W_\mu \gamma_\mu \quad (20)$$

$$\mathcal{R}_d := (1 - \beta_m) W_m \gamma_m + (1 - \beta_\mu) W_\mu \gamma_\mu \quad (21)$$

Consider following two assumptions: **A1.** mmW DL (or UL) capacity with the entire spectrum use exceeds the μ W DL

(or UL) capacity, i.e. $W_m \gamma_m > W_\mu \gamma_\mu$; and A2. the required minimum UL rate is no greater than DL rate, i.e. $\zeta \leq 1$ where ζ denotes the minimum ratio of UL to DL rates. The former A1 is justified by the motivation of the mmW use, enabling higher capacity via huge W_m that compensates low γ_m due to high distance attenuations. The later A2 is based on the well-known traffic statistics that DL demand is much higher than UL demand.

We hereafter focus on mm- μ W UL resource allocations β_m and β_μ that also determine the DL resource allocations straightforwardly as $1 - \beta_m$ and $1 - \beta_\mu$. The objective problem is then formulated as follows.

$$\begin{aligned} \text{P1. maximize } & \mathcal{R}_d \\ & \beta_m, \beta_\mu \\ \text{subject to } & \\ & \mathcal{R}_u / \mathcal{R}_d \geq \zeta \\ & 0 \leq \beta_m, \beta_\mu \leq 1. \end{aligned} \quad (22)$$

$$(23)$$

The problem above is a linear programming with two variables under a feasible region given by (22) and (23). The optimal solutions of the problem and their engineering implications are elucidated in the following section.

C. mm- μ W Resource Management

Our resource management aims at maximizing the overall mm- μ W DL rate with guaranteeing the minimum UL/DL rate ratio via adjusting mm- μ W UL allocations. The corresponding solution is provided as mmW BS-to-user density ratio $\hat{\lambda}_m$ increases.

To this end, we first divide the range of $\hat{\lambda}_m$ into the following high and low ratio regions \mathcal{C}_H and \mathcal{C}_L respectively:

$$\mathcal{C}_L := \left\{ \hat{\lambda}_m \mid \hat{\lambda}_m \leq \hat{\lambda}_\mu^* \frac{\alpha_\mu W_\mu p_L}{\zeta \alpha_m p_L W_m} \right\} \quad (24)$$

$$\mathcal{C}_H := \mathcal{C}_L^c \quad (25)$$

where the superscript c is a complement set operation. By definition, all $\hat{\lambda}_m$'s belonging to \mathcal{C}_H are larger than the values belonging to \mathcal{C}_L . These subdivided regions differentiate the optimal mm- μ W resource allocations for P1 as below.

Proposition 3. (Optimal mm- μ W UL Resource Allocations) *For a mm- μ W UDN, optimal UL allocations (β_m^*, β_μ^*) are:*

$$\begin{aligned} & \left(0, [1 + \zeta^{-1}]^{-1} \left[1 + \frac{\alpha_m W_m p_L \log \hat{\lambda}_m}{\alpha_\mu W_\mu \log \hat{\lambda}_\mu} \right] \right) \quad \text{if } \hat{\lambda}_m \in \mathcal{C}_L; \\ & \left(\left[\zeta + \frac{W_{m,u}}{W_m} \right]^{-1} \left[\zeta - \frac{\alpha_\mu W_\mu \log \hat{\lambda}_\mu}{\alpha_m W_m p_L \log \hat{\lambda}_m} \right], 1 \right) \quad \text{if } \hat{\lambda}_m \in \mathcal{C}_H. \end{aligned} \quad (26)$$

It is notable that the mm- μ W UL allocation makes a sudden change at the transition between \mathcal{C}_L and \mathcal{C}_H . The following remark specifies this behavior.

Remark 3. (μ W-to-mmW UL Allocation) *As mmW BS density increases,*

1. μ W resource should first be allocated to UL while keeping mmW dedicated to DL ($\beta_m^* = 0$);
2. mmW UL allocation begins to increase after μ W UL allocation reaches the entire spectrum ($\beta_\mu^* = 1$).

Note that such a sequential μ W-to-mmW resource allocation always occurs so long as the UL mmW bandwidth is limited, i.e. $W_{m,u} < W_m$. The remark implies allocating μ W resource more to UL than to DL for sufficiently dense mmW BS deployment. This trend is in accordance with the mm- μ W resource allocation concept from industry, where mmW spectrum is dedicated to DL transmissions while their required control signals are communicated via μ W [1].

The reasons behind, however, are distinct from each other. The approach from industry has an intention of providing stable UL communications for control signals. On the other hand, our proposed approach results from the limited mmW UL bandwidth in spite of its aiming at DL rate maximization.

Furthermore it is worth mentioning that our proposed allocation ends up with the μ W's UL dedication for extensive mmW BS proliferation. This result is in the opposite direction to the traditional μ W resource allocation trend giving top priority to DL. Preparing for the mm- μ W structure in 5G therefore may require to revisit FDD/TDD μ W DL/UL resource configurations.

Next, the tractable result in Proposition 3 provides the minimum μ W UL allocation at the initial stage of mmW UDN deployment, i.e. $\hat{\lambda}_m = 1$ since $\hat{\lambda}_m \gg 1$ by Definition 1. According to the μ W-to-mmW UL allocation order, putting $\hat{\lambda}_m = 1$ into β_μ^* for $\hat{\lambda}_m \in \mathcal{C}_L$ in (26) yields the result below.

Corollary 2. (Min. μ W UL Allocation) *The minimum μ W UL allocation amount depends solely on ζ , i.e. $\beta_\mu^* \gg 1/(1 + \zeta^{-1})$.*

The derived lower bound captures the μ W UL allocation in a nascent mmW UDN deployment. This straightforwardly accords with the resource allocation tendency in a traditional cellular network. For example, the maximum UL/DL rate ratio leads to the DL/UL equal μ W allocation, i.e. $\zeta = 1$ yielding $\beta_\mu^* = 0.5$. The minimum UL/DL rate ratio removes UL rate constraint at DL rate maximization in P1, and results in the DL dedicated allocation, i.e. $\zeta = 0$ yielding $\beta_\mu^* = 0$.

Similarly, Proposition 3 provides the maximum mmW UL allocation at the extremely dense mmW BS deployment. Applying $\hat{\lambda}_m \rightarrow \infty$ to β_m^* for $\hat{\lambda}_m \in \mathcal{C}_H$ in (26) yields such a result.

Corollary 3. (Max. mmW UL Allocation) *The maximum mmW UL allocation amount depends only on ζ , W_m , and $W_{m,u}$, i.e. $\beta_m^* \leq \left(1 + \frac{W_{m,u}}{\zeta W_m} \right)^{-1}$.*

It is remarkable that the upper bound does not depend on μ W bandwidth and SE but on mmW DL and UL bandwidths. This is because the mmW UL rate becomes dominant under this extreme mmW BS densification.

Lastly, Proposition 3 provides the blockage impact on mm- μ W resource allocations via focusing on p_L at β_μ^* for $\hat{\lambda}_m \in \mathcal{C}_L$ and β_m^* for $\hat{\lambda}_m \in \mathcal{C}_H$ in (26) as follows.

Remark 4. (Blockage Impacts on Resource Allocations) *For different geographical environments,*

1. Both mm- μ W UL allocations decrease as blockage becomes more severe;

2. The μ W UL allocation gaps between geolocations increase for $\hat{\lambda}_m \in \mathcal{C}_L$ whereas the gaps decrease for $\hat{\lambda}_m \in \mathcal{C}_H$.

The first argument results from the weak interference-limited characteristics on blockages in a UDN (see Remark 2). More blockages decrease mmW UDN SE. This results in larger DL rate decrement than UL rate due to $W_{m,u} < W_m$. As a consequence, DL/UL rate asymmetry becomes less severe.

The second argument follows from the μ W-to-mmW UL allocation order (Remark 3). For $\hat{\lambda}_m \in \mathcal{C}_L$, the mmW SE improvement by densification amplifies the blockage dependent impact on the SE, leading to the result. For $\hat{\lambda}_m \in \mathcal{C}_H$, on the other hand, mmW BS densification becomes almost always achieving LOS conditions, i.e. $p_L \rightarrow 1$, and therefore the blockage impact on SE rapidly diminishes. Fig. 7 in Section V-C illustrates such a blockage dependent behavior.

The optimal mm- μ W UL allocations in Proposition 3 are followed by the maximized DL rate with the minimum UL constraint (22) in P1 as below.

Proposition 4. (Max. DL UDN Rate) *For a mm- μ W UDN with the optimal UL allocation given in Proposition 3, the maximized DL rate \mathcal{R}_d^* is:*

$$\begin{aligned} & [2(\zeta + 1)]^{-1} \log \hat{\lambda}_\mu^{\alpha_\mu W_\mu} \hat{\lambda}_m^{\alpha_m W_m p_L} & \text{if } \hat{\lambda}_m \in \mathcal{C}_L; \\ & \left[2 \left(\zeta + \frac{W_{m,u}}{W_m} \right) \right]^{-1} \log \hat{\lambda}_\mu^{\alpha_\mu W_\mu} \hat{\lambda}_m^{\alpha_m W_{m,u} p_L} & \text{if } \hat{\lambda}_m \in \mathcal{C}_H. \end{aligned} \quad (27)$$

The result shows that the maximized DL rate is a logarithmic function of mm- μ W BS-to-user densities. It is remarkable that the maximized DL rate becomes highly restricted by the limited UL bandwidth $W_{m,u}$ for $\hat{\lambda}_m \in \mathcal{C}_H$. The following subsection proposes mmW UL decoupling that relieves the UL rate bottleneck, thereby ensuring scalable DL rate.

D. mm- μ W Resource Management with mmW UL Decoupling

To resolve this UL bottleneck, we propose a novel mmW UL decoupling scheme that enables mmW UL receptions at the incumbent μ W BSs. By the aid of this proposed approach, mmW UL users are able to associate with not only mmW but also μ W BSs. Its resultant UL BS densification as a result increases the overall UL rate under a UDN regime, leading to ease the UL bottleneck. Note that DL and UL are decoupled over different μ -mmW RATs in the proposed scheme. The association distance reduction via obtaining more UL BSs is the sole advantage of the scheme. It is thus different from μ W single RAT UL/DL decoupling [34] that resolves the DL/UL imbalance in transmission power and/or scheduling, of which the both mismatches are negligible under an interference-limited UDN (see Definition 1 and discussion after Remark 2).

From a practical point of view, such a mmW UL decoupling is cost-effective. The approach only requires additional mmW receive antennas with ADC at μ W BSs. Sharing the existing data backhauls while having no need of power amplifiers as well as the additional site acquisition cost are expected to make the solution practically viable.

To analyze the impact of mmW UL decoupling, we define the following mmW BS-to-user density ratio region.

$$\mathcal{D} := \left\{ \hat{\lambda}_m \mid \hat{\lambda}_\mu + \hat{\lambda}_m \geq \hat{\lambda}_m \frac{W_m}{W_{m,u}} \right\} \quad (28)$$

This region implies an extreme case where the increased number of mmW UL receivable BSs with mmW UL decoupling (LHS of the inequality in (28)) dominate the limited UL bandwidth (RHS in (28)). The mm- μ W resource allocations when mmW BS-to-user density ratio belongs to this region therefore show different tendency from the allocations without mmW UL decoupling as follows.

Proposition 5. (Optimal mm- μ W UL Resource Allocations with mmW UL Decoupling) *For a mm- μ W UDN with mmW UL decoupling, optimal UL allocations (β_m^*, β_μ^*) are:*

$$\begin{aligned} & \left(0, [1 + \zeta^{-1}]^{-1} \left[1 + \frac{\alpha_m W_m p_L \log \hat{\lambda}_m}{\alpha_\mu W_\mu \log \hat{\lambda}_\mu} \right] \right) & \text{if } \hat{\lambda}_m \in \mathcal{C}_L \cap \mathcal{D}^c; \\ & \left(\left[\zeta + \frac{W_{m,u} \log(\hat{\lambda}_m + \hat{\lambda}_\mu)}{W_m \log \hat{\lambda}_m} \right]^{-1} \left[\zeta - \frac{\alpha_\mu W_\mu \log \hat{\lambda}_\mu}{\alpha_m W_m p_L \log \hat{\lambda}_m} \right], 1 \right) & \text{if } \hat{\lambda}_m \in \mathcal{C}_H \cap \mathcal{D}^c; \\ & \left(\left[1 + \frac{W_{m,u} \log(\hat{\lambda}_m + \hat{\lambda}_\mu)}{\zeta W_m \log \hat{\lambda}_m} \right]^{-1} \left[1 + \frac{\alpha_\mu W_\mu \log \hat{\lambda}_\mu}{\alpha_m W_m p_L \log \hat{\lambda}_m} \right], 0 \right) & \text{if } \hat{\lambda}_m \in \mathcal{D}. \end{aligned} \quad (29)$$

The resource allocation impact of mmW UL decoupling compared to the allocations without the decoupling is specified in the following remark.

Remark 5. (mmW UL Decoupling Impact on Resource Allocations) *The impact of mmW UL decoupling on mm- μ W UL resource allocations for different mmW BS densities is as follows:*

1. For high mmW BS densification ($\hat{\lambda}_m \in \mathcal{C}_H \cap \mathcal{D}^c$), mmW UL decoupling reduces the mmW UL allocation;
2. For the moderate densification ($\hat{\lambda}_m \in \mathcal{D}$), UL transmissions become relying only on mmW while keeping μ W dedicated to DL, which is completely opposite of what mm- μ W resources allocate to in the case without the decoupling; and
3. For the low densification ($\hat{\lambda}_m \in \mathcal{C}_L \cap \mathcal{D}^c$), mmW decoupling does not affect the mm- μ W resource allocations.

It is worth noticing that the second argument shows the opposite trend of mm- μ W resource allocation. This results from the situation where the decoupling effect in the aggregate mmW UL receivable BS densification that overcomes the mmW UL spectrum limitation. It makes mmW dedicated to UL, resolving UL rate bottleneck more effectively than the μ W's UL dedication while improving DL rate in so doing.

In addition, the DL rate resulting from the mm- μ W allocation in Proposition 5 is presented as below.

Proposition 6. (Max. DL UDN Rate with mmW UL Decoupling) *For a mm- μ W UDN with mmW UL decoupling and the optimal UL allocation given in Proposition 5, maximized DL*

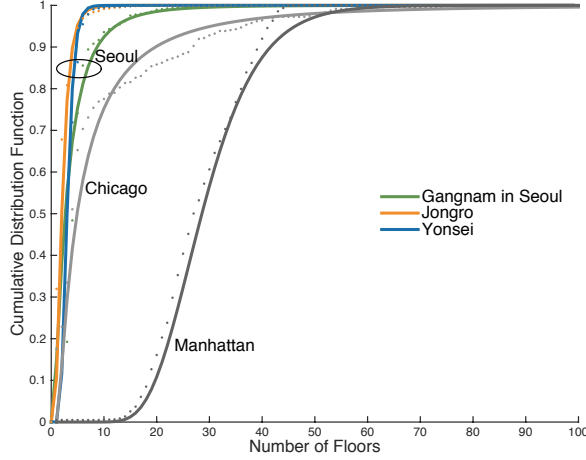


Fig. 5. Distributions of the number of floors in Seoul, Korea (dotted lines), and their lognormal fitted curves (solid lines). The root mean square error of each fitted curve is less than 0.016.

rate \mathcal{R}_d^* is:

$$\begin{aligned}
 & [2(1 + \zeta)]^{-1} \log \hat{\lambda}_\mu^{\alpha_\mu W_\mu} \hat{\lambda}_m^{\alpha_m W_m PL} \quad \text{if } \hat{\lambda}_m \in \mathcal{C}_L \cap \mathcal{D}^c; \\
 & \left[2 \left(\zeta + \frac{W_{m,u} \log(\hat{\lambda}_m + \hat{\lambda}_\mu)}{W_m \log \hat{\lambda}_m} \right) \right]^{-1} \log \hat{\lambda}_\mu^{\alpha_\mu W_\mu} (\hat{\lambda}_m + \hat{\lambda}_\mu)^{\alpha_m W_{m,u} PL} \quad \text{if } \hat{\lambda}_m \in \mathcal{C}_H \cap \mathcal{D}^c; \\
 & \left[2 \left(1 + \frac{\zeta W_m \log \hat{\lambda}_m}{W_{m,u} \log(\hat{\lambda}_m + \hat{\lambda}_\mu)} \right) \right]^{-1} \log \hat{\lambda}_\mu^{\alpha_\mu W_\mu} \hat{\lambda}_m^{\alpha_m W_{m,u} R_L} \quad \text{if } \hat{\lambda}_m \in \mathcal{D}.
 \end{aligned} \tag{30}$$

This DL rate with mmW decoupling and its improvement from the DL rate without the decoupling are visualized at Fig. 9 in Section V-C.

V. NUMERICAL EVALUATION WITH A REAL GEOGRAPHY BASED 3D BLOCKAGE MODEL

The mm- μ W SEs in Section III and the corresponding DL/UL resource management in Section IV are numerically evaluated in this section. To maximize their practical feasibility, we apply a 3D blockage model, and calculate average LOS distance R_L with the actual building geography in Seoul, Korea.

A. Average LOS Distance under a Real Geography Based 3D Blockage Model

The possibility that a given link with distance r is LOS not only depends on blockage locations but also their heights. We consider both effects by applying a 3D blockage model [12]. Its corresponding 3D average LOS distance is given as:

$$R_L = \frac{2(1 - \kappa)}{\beta\eta} \tag{31}$$

where

$$\beta := \frac{-2\rho \log(1 - \kappa)}{\pi A}, \tag{32}$$

$$\eta := \int_0^1 \Pr(H \leq (1 - s)B) ds, \tag{33}$$

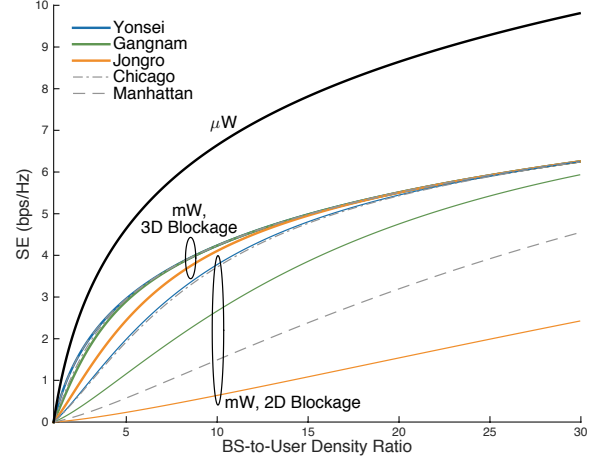


Fig. 6. The spectral efficiencies of DL μ W and DL mmW with the 2D/3D LOS distance values at Gangnam, Jongro, Yonsei in Seoul, Korea as well as Manhattan and Chicago in the US where the LOS distance values are found in Table I ($\alpha_\mu = 4$, $\alpha_m = 2.5$, $\lambda_u = 1$).

ρ average blockage perimeter, κ average building coverage, A average building area, H building height, and B BS height. Note that putting $\eta = 1$ into (33) yields 2D average LOS distance R_L^{2D} .

By the aid of the ministry of land, infrastructure, and Transport of Korea, we calculate β and η that correspond to three hotspot regions in Seoul, Korea: Gangnam, Jongro, and Yonsei university town, visualized in Fig. 4. The results are presented in Table I. Comparing 2D and 3D LOS distances reveals that these two values are less correlated. For instance, the R_L^{2D} in Gangnam is larger than the value in Manhattan, but such a relationship is reversed from the perspective of R_L . It is thus necessary to consider a 3D blockage model for a practically feasible analysis.

The calculations of β rely on QGIS, an open source geographic information system (GIS) [35]. The process for η additionally requires the distribution of building height H due to (33). Now that the given geographic data does not include the building height information, we detour this problem via the information on the number of building floors. We assume unit floor height is 3 m, and then derive the building floor distribution via the data curve fitting (see Fig. 5). For BS heights, also required in (33), we assume each BS height follows the average building height EH . Note that the η values of Manhattan and Chicago are also calculated in this work for fair comparisons of the blockage environments. Their geographical data follow from the same sources in [29].

B. mm- μ W SEs under a Real Geography Based 3D Blockage Model

Based on a 3D blockage model with the actual building statistics summarized in Table I, Fig. 6 visualizes the mm- μ W SEs in Theorems 1 and 2. The significant gap between mm- μ W UDN SEs can be explained via the effects of path loss exponent and mmW blockages in a weak interference-limited regime. The smaller mmW path loss exponent for LOS links



Fig. 4. Target areas for building statistics: Gangnam, Jongro, and Yonsei, Seoul, Korea.

TABLE I
AVERAGE LOS DISTANCES MEASURED FROM BUILDING STATISTICS IN SEOUL, KOREA

Building parameters (unit)	Gangnam ($2 \times 2 \text{ km}^2$)	Jongro ($1 \times 1 \text{ km}^2$)	Yonsei ($2 \times 2 \text{ km}^2$)	Manhattan [29] ($1 \times 1 \text{ km}^2$)	Chicago [29] ($0.5 \times 0.5 \text{ km}^2$)
Average perimeter ρ (m ²)	59.02	39.29	51.99	73.78	114.48
Average area A (m ²)	218.60	107.67	173.95	312.26	886.46
Coverage κ (%)	34.77	46.90	25.48	45.83	42.02
Average height EH (m)	14.23	8.12	11.14	101.00	28.95
Height $\sim \log\mathcal{N}(\mu, \sigma)$	(1.62, 0.27)	(0.69, 0.55)	(1.10, 0.34)	(3.32, 0.30)	(1.36, 1.23)
2D blockage parameter β	0.073	0.014	0.056	0.092	0.045
3D height parameter η	0.36	0.22	0.13	0.12	0.46
2D LOS distance R_L^{2D} (m)	17.77	7.22	26.63	11.75	25.88
3D LOS distance R_L (m)	49.61	33.33	198.76	98.11	56.20

results in the lower mmW SE than μ W SE. Further mmW SE degradation results from the more blockages than the μ W environment that is blockage-free as assumed in Section II-B.

Another notable point is the impact of 3D blockage model whose resultant mmW SEs are higher than the values under a 2D blockage model. At a receiver in the 2D model, all buildings whose locations are in the straight line from the transmitter become blockages. In the 3D model, on the other hand, different building heights make some of these buildings still guarantee LOS conditions. Such effects reduces blockage degradations compared to the 2D model, thereby yielding higher SEs.

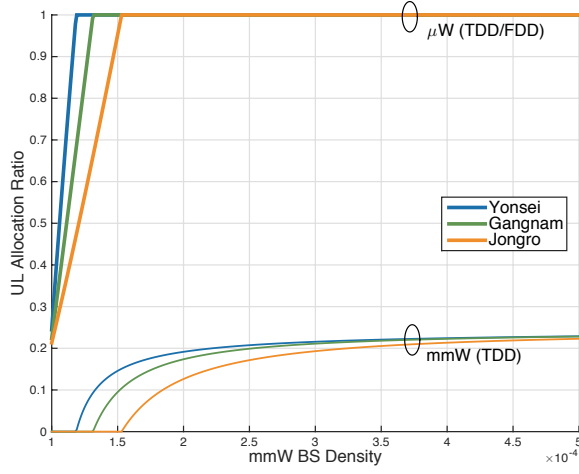
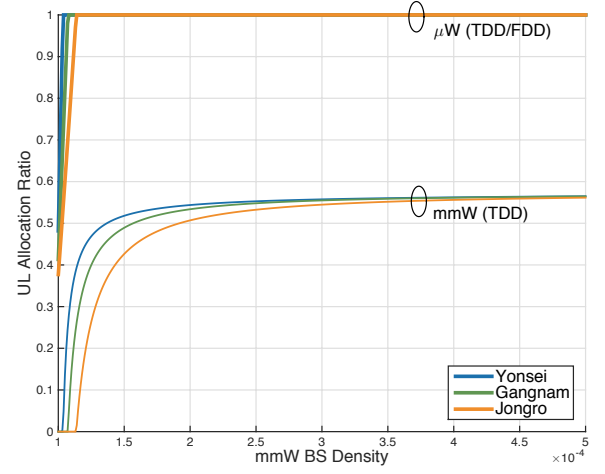
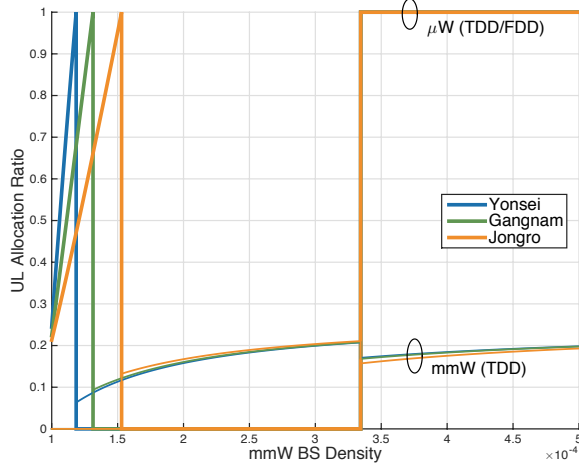
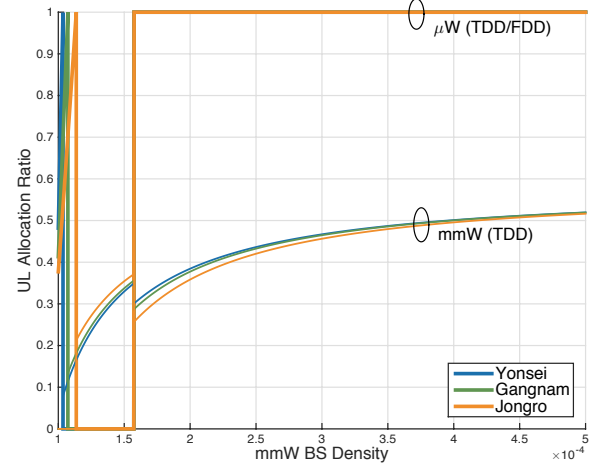
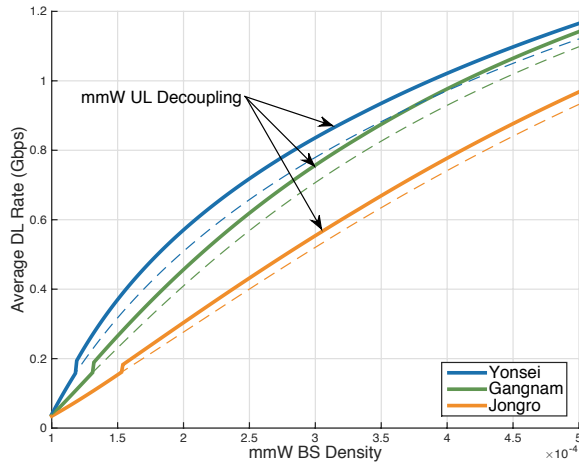
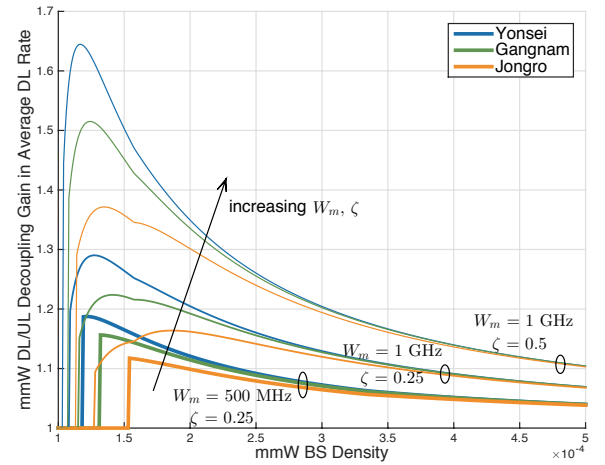
C. mm- μ W Resource Management and mmW UL Decoupling Impact

We by default consider mm- μ W bandwidths are respectively given as 500 and 20 MHz under 25% minimum UL/DL rate ratio. The corresponding result is compared with the case where mmW bandwidth is set as 1 GHz under the 50% UL/DL rate ratio. Note that such UL/DL rate ratios are in line with the 3GPP Release 12 standards [36]: for its peak rate specifications, the UL/DL rate ratio 25% indicates user equipment category (CAT) 5, 10, and 14; the ratio 50% is in

accordance with CAT 1–3, and 8, where the ratio for smart devices ranges from 8% to 50%.

Fig. 7 visualizes mm- μ W UL allocations without mmW UL decoupling (see Proposition 3 for analytic details). As mmW BS density increases, it shows μ W UL allocation increases while keeping mmW dedicated to DL. According to Fig. 7-a, this allocation trend holds until less than 1.5 times (or 1.2 times under different settings in Fig. 7-b) mmW BS densification compared to user density, where the entire μ W bandwidth starts dedicating to UL. After reaching the UL dedication of μ W, mmW UL allocation then begins to increase (Remark 3). The minimum μ W UL allocation is only a function of the minimum UL/DL rate ratio (Corollary 2). The UL/DL rate ratio also determines the maximum mmW UL allocation, in conjunction with the available mmW DL/UL bandwidths (Corollary 3). Note that these minimum μ W and maximum mmW UL allocations are independent of blockages. In the allocation range excluding these two extreme cases, less severe blockages (average LOS distance: Yonsei < Gangnam < Jongro) require more mm- μ W UL allocations (Remark 4). It follows from the fact that reducing blockages improves DL rate more than UL rate due to the limited UL bandwidth $W_{m,u} < W_m$.

Fig. 8 illustrates the impact of mmW UL decoupling on

(a) For $W_m = 500$ MHz, $\zeta = 0.25$ (b) For $W_m = 1$ GHz, $\zeta = 0.5$ Fig. 7. Optimal mm- μ W UL resource allocations ($W_\mu = 20$ MHz, $\lambda_u = 10^{-4}$, $\lambda_\mu = 2 \times 10^{-4}$, $f_s = 244.14$ kHz, $\delta = 10$ dB, $\epsilon = 0.7$).(a) For $W_m = 500$ MHz, $\zeta = 0.25$ (b) For $W_m = 1$ GHz, $\zeta = 0.5$ Fig. 8. Optimal mm- μ W UL resource allocations with mmW UL decoupling ($W_\mu = 20$ MHz, $\lambda_u = 10^{-4}$, $\lambda_\mu = 2 \times 10^{-4}$, $f_s = 244.14$ kHz, $\delta = 10$ dB, $\epsilon = 0.7$).(a) Maximized average DL rate ($W_m = 500$ MHz, $\zeta = 0.25$)

(b) Average DL rate gain by mmW UL decoupling

Fig. 9. Maximized average DL rate and the effect of mmW UL decoupling ($W_\mu = 20$ MHz, $\lambda_u = 10^{-4}$, $f_s = 244.14$ kHz, $\delta = 10$ dB, $\epsilon = 0.7$).

mm- μ W UL resource allocations (Proposition 5). As shown in Fig. 8-a, the proposed decoupling reduces mmW UL allocation for the mmW BS-to-user density ratio larger than 3.3 (or 1.6 in Fig. 8-b). For the mmW BS-to-user density in the range of 1.5 to 3.3 (or 1.1 to 1.6 in 8-b), the proposed technique makes UL transmissions counting solely on mmW instead of μ W since the decoupled mmW UL BS density overcompensates the limited mmW UL bandwidth $W_{m,u}$ (Remark 5).

Fig. 9 shows the impact of mmW UL decoupling on the overall DL rate. To be specific, the maximized DL rate corresponding to the proposed mm- μ W resource management is presented in Fig. 9-a. According to Fig. 9-b, mmW UL decoupling is more beneficial for large mmW bandwidth and/or the minimum UL/DL rate ratio. For the given scenarios with mmW UL decoupling, maximized DL rate improves up to 1.65 times.

VI. CONCLUSION

This paper tackles the mmW UL bottleneck due to high PAPR in 5G mm- μ W cellular networks. As its solution, inter-tier DL/UL resource management in concert with mmW UL decoupling is proposed, and its impact is analyzed in a tractable manner. The result indicates that mm- μ W resource allocations have high priorities respectively in DL and UL (Proposition 3). In addition, it shows mmW UL decoupling mitigates the UL bottleneck, thereby increasing DL rate (Proposition 6). The closed-form mm- μ W UDN SEs (Theorems 1 and 2) are key enablers to provide such an intuitive guideline. A real geography based 3D blockage model enhances the practical feasibility of our analysis.

The tractable analysis of this study removes the complicated representations in mm- μ W resource management, yet in return reduces its practical viability. To further validate our result, its follow-up investigation may incorporate more realistic near-field channel behaviors. 3D channel characteristics and diverse path loss attenuations are major candidates.

Further extension could also contemplate the impact of DL transmission outage. Our mm- μ W resource management in the end suggests mmW exclusive DL transmissions from the average DL rate point of view. The blockage vulnerable nature of mmW, however, makes it incapable of supporting ultra-low latency applications such as the tactile internet. The complementary DL use of μ W when encountering blockages can be its possible solution. Analyzing such a microscopic operation in view of the mm- μ W resource allocations is another interesting topic for future work.

APPENDIX I. PROOF OF LEMMAS

A. Proof of Lemma 1 (Homogeneous Active BS Approximation)

Consider the Voronoi cell size distribution [37] where the cell size is normalized by BS density. Restoring BS density λ rephrases the cell size probability density distribution as

$$f_X(x) = \frac{3.5^{3.5}}{\Gamma(3.5)} \lambda^{4.5} x^{3.5} e^{-3.5\lambda x} \quad (34)$$

where X denotes the cell size. The variance of Voronoi cell sizes is then represented as follows.

$$\text{Var}(X) = EX^2 - (EX)^2 = \frac{5.5 \times 4.5}{3.5^2 \lambda^2} - \left(\frac{4.5^2}{3.5 \lambda} \right)^2 \quad (35)$$

$$= \frac{4.5}{3.5^2 \lambda^2} \quad (36)$$

As λ (or $\hat{\lambda}$) goes to infinity, (36) approaches zero, indicating location dependency of the activation (or cell size) marks becomes negligible. If users are uniformly distributed, this makes the active BS PPP be regarded as a homogeneous PPP that is independently thinned by p_a . Applying Taylor expansion to p_a for $\hat{\lambda} \rightarrow \infty$ yields $p_a = \hat{\lambda}^{-1}$, and thus the resultant homogeneous PPP density $p_a \lambda$ converges to λ_u . ■

B. Proof of Lemma 2 (UDN Approximation)

Applying the nearest BS distance distribution [38],

$$E_R [\exp(-\lambda_u \pi r^2 I)] = 2\lambda \pi \int_{r>0} r \exp\{-\lambda \pi r^2 - \lambda_u \pi r^2 I\} dr \quad (37)$$

$$= [1 + \hat{\lambda}^{-1} I]^{-1}. \quad (38)$$

Exploiting Taylor expansion while preventing negative values completes the proof. ■

C. Proof of Lemma 3 (μ W Interference Constant Bounds)

The proof of the upper bound is trivial when recalling ρ_μ 's integration range that is larger than the range of $\rho_\mu^{(t)}$. For the lower bound, applying Taylor expansion at the integrand in $\rho_\mu^{(t)}$ yields

$$\rho_\mu^{(t)} \geq \int_{u>(e^t-1)^{-\frac{2}{\alpha_\mu}}} \left(1 - u^{\frac{\alpha_\mu}{2}}\right)^+ du \quad (39)$$

$$= \left(1 + \frac{2}{\alpha_\mu}\right)^{-1} \left[1 + (e^t - 1)^{-\left(1 + \frac{2}{\alpha_\mu}\right)}\right] - (e^t - 1)^{-\frac{2}{\alpha_\mu}} \quad (40)$$

$$\geq \left(1 + \frac{2}{\alpha_\mu}\right)^{-1} - (e^t - 1)^{-\frac{2}{\alpha_\mu}} \quad (41)$$

from which the result follows. ■

D. Proof of Lemma 4 (Directional Interference Thinning)

Consider the DL aggregate interference at a typical user.

$$I_{\Sigma_{m,d}} := \sum_{i \in \Phi_m} \Theta_i g_i r_i^{-\alpha_m} \mathbf{1}_{R_L}(r_i) \quad (42)$$

$$\stackrel{(a)}{\approx} \sum_{i \in \Phi_m(p_m \lambda_m)} \Theta_i g_i r_i^{-\alpha_m} \mathbf{1}_{R_L}(r_i) \quad (43)$$

$$\stackrel{(b)}{=} \sum_{i \in \Phi_m\left(p_m \lambda_m \left(\frac{\theta}{2\pi}\right)^{\frac{2}{\alpha_m}}\right)} g_i r_i^{-\alpha_m} \mathbf{1}_{R_L}(r_i) \quad (44)$$

where (a) follows from Lemma 1 and (b) from: (i) $E\Theta_i = \frac{\theta}{2\pi}$ due to uniformly distributed users and (ii) mapping theorem, also known as displacement theorem [38]. The UL aggregate interference representation follows the same procedure. ■

$$\gamma_{\mu,d} \geq \log \left(1 + \left[\rho_{\mu}^{-1} \hat{\lambda}_{\mu} \right]^{\frac{\alpha_{\mu}}{2}} \right) + \underbrace{\frac{\alpha_{\mu}}{2} \left[\rho_{\mu} \hat{\lambda}_{\mu}^{-1} - \left(1 + \hat{\lambda}_{\mu}^{-\frac{\alpha_{\mu}}{2}} \right)^{\frac{2}{\alpha_{\mu}}} {}_2F_1 \left(-\frac{2}{\alpha_{\mu}}, -\frac{2}{\alpha_{\mu}}; 1 - \frac{2}{\alpha_{\mu}}; \frac{1}{1 + \hat{\lambda}_{\mu}^{\frac{\alpha_{\mu}}{2}}} \right) \right]}_{(b)} \quad (53)$$

$$\gamma_{\mu,d} \leq \left(1 - \hat{\lambda}_{\mu}^{-1} \right) \int_{t>0} \left[1 - \left(\hat{\lambda}_{\mu} - 1 \right)^{-1} \frac{\alpha_{\mu}}{\alpha_{\mu} + 2} (e^t - 1)^{\frac{2}{\alpha_{\mu}}} \right]^+ dt \quad (54)$$

$$\begin{aligned} &= \left(1 - \hat{\lambda}_{\mu}^{-1} \right) \log \left(1 + \left[\left(\hat{\lambda}_{\mu} - 1 \right) \left(1 + \frac{2}{\alpha_{\mu}} \right)^{\frac{\alpha_{\mu}}{2}} \right] \right) - \frac{\hat{\lambda}_{\mu}}{\left(\hat{\lambda}_{\mu} - 1 \right)^2} \left\{ \frac{2}{\alpha_{\mu}} + \left(\frac{2}{\alpha_{\mu}} \right)^2 \right\}^{-1} \\ &\times \left[\rho_{\mu} - \left\{ 1 + \left[\left(1 + \frac{2}{\alpha_{\mu}} \right) \left(\hat{\lambda}_{\mu} - 1 \right)^{\frac{\alpha_{\mu}}{2}} \right]^{\frac{2}{\alpha_{\mu}}} \right\} {}_2F_1 \left(-\frac{2}{\alpha_{\mu}}, -\frac{2}{\alpha_{\mu}}; 1 - \frac{2}{\alpha_{\mu}}; \left\{ 1 + \left[\left(1 + \frac{2}{\alpha_{\mu}} \right) \left(\hat{\lambda}_{\mu} - 1 \right)^{\frac{\alpha_{\mu}}{2}} \right]^{\frac{2}{\alpha_{\mu}}} \right\}^{-1} \right) \right] \end{aligned} \quad (55)$$

(c)

E. Proof of Lemma 5 (mmW Interference Constant Bounds)

The upper bound is straightforwardly derived when comparing the integration ranges of $\rho_m^{(t)}$ and ρ_m . For the lower bound, applying Taylor expansion at the integrand of $\rho_m^{(t)}$ yields

$$\rho_m^{(t)} \geq \int_{(e^t-1)^{-\frac{2}{\alpha_m}}}^{\min \left\{ 1, \left(\frac{R_L}{r} \right)^2 (e^t-1)^{-\frac{2}{\alpha_m}} \right\}} \left(1 - u^{\frac{\alpha_m}{2}} \right) du. \quad (45)$$

Assume the upper limit of the integration in (45) becomes 1, yielding

$$\rho_m^{(t)} \geq 1 - (e^t - 1)^{-\frac{2}{\alpha_m}} - \left(1 + \frac{\alpha_m}{2} \right)^{-1} \left[1 - (e^t - 1)^{-\frac{2}{\alpha_m} - 1} \right] \quad (46)$$

$$\geq 1 - (e^t - 1)^{-\frac{2}{\alpha_m}} - \left(1 + \frac{\alpha_m}{2} \right)^{-1}. \quad (47)$$

Consider the integration upper limit in (45) becomes 1 with probability no less than $1 - \varepsilon$ for a constant $\varepsilon > 0$, i.e.

$$\Pr \left(R \leq R_L (e^t - 1)^{-\frac{1}{\alpha_m}} \right) = 1 - e^{-\lambda_m \pi R_L^2 (e^t - 1)^{-\frac{2}{\alpha_m}}} \geq 1 - \varepsilon. \quad (48)$$

It is rephrased by

$$t \leq \log \left[1 + \left(\frac{\lambda_m \pi R_L^2}{\log \varepsilon^{-1}} \right)^{\frac{\alpha_m}{2}} \right]. \quad (49)$$

For $\lambda_m \rightarrow \infty$, the inequality (49) always holds for all t , resulting in the first argument of the lemma. For a UDN, when applying Lemma 2 to (9), the value t is upper bounded by $\log \left[1 + \left(\frac{\lambda_m}{\rho_m \lambda_u} \right)^{\frac{\alpha_m}{2}} \right]$. Making this upper bound belong to the inequality in (49) is identical to satisfying (49) for all t . This leads to $\varepsilon \geq e^{-\rho_m \lambda_u \pi R_L^2}$. Taking the minimum value of ε completes the proof. ■

APPENDIX II. PROOFS OF PROPOSITIONS

A. Proof of Proposition 1 (μ W DL/UL SE Bounds)

According to Lemma 1, interferer PPPs for DL Φ_{μ} and for UL Φ_{μ} in a UDN can be regarded as independently thinned homogeneous PPPs respectively from Φ_{μ} and Φ_u . For DL μ W UDN SE at a typical user, the interferer density is then given as $p_a \lambda_{\mu} P_{\mu,d}^{\frac{2}{\alpha_{\mu}}} \approx \lambda_u P_{\mu,d}^{\frac{2}{\alpha_{\mu}}}$ where the approximation results from Taylor expansion for a UDN. Note that $P_{\mu,d}^{\frac{2}{\alpha_{\mu}}}$ follows from mapping theorem [38] that interchanges P times power

increase with $P^{\frac{2}{\alpha}}$ times density increase. Similarly, the density of the desired BS, denoting the associated BS transmitting the desired DL signal, is represented by $\lambda_{\mu} P_{\mu,d}^{\frac{2}{\alpha_{\mu}}}$ thanks to mapping theorem.

Starting from this setting, applying the equation (16) in [32] with minor modification yields the μ W DL UDN SE $\gamma_{\mu,d}$ as

$$\gamma_{\mu,d} = \int_{t>0} \mathbb{E}_{\Phi_{\mu}} [\Pr \{ \log(1 + \text{SIR}_{\mu,d}) \geq t \}] dt \quad (50)$$

$$= \int_{t>0} \mathbb{E}_R \left[\exp \left(-\pi r^2 \rho_{\mu}^{(t)} \lambda_u P_{\mu,d}^{\frac{2}{\alpha_{\mu}}} (e^t - 1)^{\frac{2}{\alpha_{\mu}}} \right) \right] dt \quad (51)$$

$$\stackrel{(a)}{\approx} \int_{t>0} \left[1 - \rho_{\mu}^{(t)} \hat{\lambda}_{\mu}^{-1} (e^t - 1)^{\frac{2}{\alpha_{\mu}}} \right]^+ dt \quad (52)$$

where (a) follows from Lemma 2 and the probability density function (pdf) of the BS-to-user association distance R :

$$f_R(r) = 2\pi r \lambda_{\mu} P_{\mu,d}^{\frac{2}{\alpha_{\mu}}} e^{-\pi r^2 \lambda_{\mu} P_{\mu,d}^{\frac{2}{\alpha_{\mu}}}}.$$

Applying the upper bound of $\rho_{\mu}^{(t)}$ in Lemma 3 leads to the lower bound of $\gamma_{\mu,d}$ as (53) at the top of this page, where Gaussian hypergeometric function ${}_2F_1(a, b; c; z) := \sum_{k=0}^{\infty} \frac{z^k a^{(k)} b^{(k)}}{k! c^{(k)}}$, and $x^{(k)}$ rising factorial. The function (b) monotonically decreases with $\hat{\lambda}_{\mu}$ for all $\alpha_{\mu} > 2$, having its maximum ρ_{μ} and minimum 1 respectively at $\hat{\lambda}_{\mu} = 0$ and $\hat{\lambda}_{\mu} \rightarrow \infty$ [39]. Considering $\hat{\lambda}_{\mu} \gg 1$ yields the desired DL μ W UDN SE lower bound.

In a similar manner, applying the lower bound of $\rho_{\mu}^{(t)}$ in Lemma 3 results in the upper bound of $\gamma_{\mu,d}$ as (55) at the top of the page. The function (c) monotonically decreases with $\hat{\lambda}_{\mu}$ for all $\hat{\lambda}_{\mu} \geq 1$ and $\alpha_{\mu} > 2$, having its maximum ρ_{μ} and minimum 1 respectively at $\hat{\lambda}_{\mu} = 1$ and $\hat{\lambda}_{\mu} \rightarrow \infty$ [39]. Considering $\hat{\lambda}_{\mu} \gg 1$ leads to the desired DL μ W UDN SE upper bound.

For UL μ W UDN SE at a typical BS, the interferer and the desired BS densities are respectively represented as $p_s \lambda_u P_{\mu,u}^{\frac{2}{\alpha_{\mu}}} \approx \lambda_u P_{\mu,u}^{\frac{2}{\alpha_{\mu}}}$ and $\lambda_{\mu} P_{\mu,u}^{\frac{2}{\alpha_{\mu}}}$ due to mapping theorem [38] and Taylor expansion. When noticing the $P_{\mu,d}^{\frac{2}{\alpha_{\mu}}}$'s of the interferer and the desired BS are cancelled out in (52), such an UL and DL transmitting power difference in the interferer and the desired BS densities do not affect the SE calculation afterwards. As a consequence, UL μ W UDN SE shares the same lower and upper bound with the DL case,

$$\gamma_{m,d} \leq \left(1 - \frac{1}{\hat{\lambda}_m}\right) \int_{t>0} \left(1 - e^{-\lambda_m \pi R_L^2 \left\{1 + \frac{1}{\hat{\lambda}_m} \left[1 - \left(1 + \frac{\alpha_m}{2}\right)^{-1}\right] \left[\frac{\theta(e^t - 1)}{2\pi}\right]^{\frac{2}{\alpha_m}}\right\}}\right) \left\{1 - \left[(\hat{\lambda}_m - 1) \left(1 + \frac{2}{\alpha_m}\right)\right]^{-1} \left[\frac{\theta(e^t - 1)}{2\pi}\right]^{\frac{2}{\alpha_m}}\right\}^+ dt \quad (60)$$

$$\stackrel{(a)}{\leq} \left(1 - \frac{1}{\hat{\lambda}_m}\right) \int_{t>0} p_L^{(t)} \left[1 - \left[(\hat{\lambda}_m - 1) \left(1 + \frac{2}{\alpha_m}\right)\right]^{-1} \left[\frac{\theta(e^t - 1)}{2\pi}\right]^{\frac{2}{\alpha_m}}\right]^+ dt \quad (61)$$

completing the proof. \blacksquare

B. Proof of Proposition 2 (mmW DL/UL SE Bounds)

In a similar procedure to the proof of Proposition 1, the interferer PPP for DL Φ_m is approximated by a homogeneous PPP with density $\lambda_u \left(\frac{P_{m,d}\theta}{2\pi}\right)^{\frac{2}{\alpha_m}}$, and for UL Φ_u by also a homogeneous PPP with density $\lambda_u \left(\frac{P_{m,u}\theta}{2\pi}\right)^{\frac{2}{\alpha_m}}$ according to Lemmas 1 and 4 with exploiting Taylor expansion under a UDN regime. For DL mmW SE, the desired BS density is represented as $\lambda_m P_{m,d}^{\frac{2}{\alpha_m}}$, yielding

$$\gamma_{m,d} = \int_{t>0} \mathbb{E}_{\Phi_m} [\Pr\{\log(1 + \text{SIR}_{m,d}) \geq t\}] dt \quad (56)$$

$$= \int_{t>0} \mathbb{E}_R \left[\exp \left(-\pi r^2 \rho_\mu^{(t)} \lambda_u \left(\frac{\theta}{2\pi} P_{m,d} \right)^{\frac{\alpha_\mu}{2}} (e^t - 1)^{\frac{2}{\alpha_m}} \right) \right] dt \quad (57)$$

$$= 2\pi \lambda_m P_{m,d}^{\frac{2}{\alpha_m}} \int_{t>0} \int_0^{R_L} r \exp \left\{ -\pi r^2 \lambda_m P_{m,d}^{\frac{2}{\alpha_m}} - \rho_\mu^{(t)} \lambda_u P_{m,d}^{\frac{2}{\alpha_\mu}} \pi r^2 \left[\frac{\theta}{2\pi} (e^t - 1) \right]^{\frac{2}{\alpha_m}} \right\} dr dt \quad (58)$$

where the last result comes from the pdf of R : $f_R(r) = 2\pi r \lambda_m P_{m,d}^{\frac{2}{\alpha_m}} e^{-\pi r^2 \lambda_m P_{m,d}^{\frac{2}{\alpha_m}}}$.

Applying the upper bound in Lemma 5 results in the lower bound of DL mmW SE as below.

$$\gamma_{m,d} \geq \int_{t>0} p_L^{(t)} \left[1 + \hat{\lambda}_m^{-1} \rho_m \left[\frac{\theta}{2\pi} (e^t - 1) \right]^{\frac{2}{\alpha_m}} \right]^{-1} dt \quad (59)$$

Next, exploiting the lower bound in Lemma 5 yields the upper bound of DL mmW SE as (61) at the top, where (a) follows from $\rho_m \geq 1 - \left(1 + \frac{\alpha_m}{2}\right)^{-1}$. Considering $\hat{\lambda}_\mu \gg 1$ yields the desired DL mmW SE upper bound.

As in the case of the proof of Proposition 1, the transmitting power effects at the desired signal and interference are mutually cancelled out after (58). It makes the lower and upper bounds of DL and UL be identical, finalizing the proof. \blacksquare

C. Proof of Proposition 3 (Optimal mm- μ W UL Resource Allocations)

Consider \mathcal{R}_d in (21) that is rephrased by

$$\beta_\mu = -c_1 \beta_m + (c_2 - \mathcal{R}_d) \quad (62)$$

where $c_1 := W_m \gamma_m / (W_\mu \gamma_\mu)$ and $c_2 := W_m \gamma_m + W_\mu \gamma_\mu$. Note that $c_2 \geq \mathcal{R}_d$ since c_2 is the maximum DL rate achieved

when the entire mm- μ W resource are dedicated to DL. The minimum UL/DL rate ratio in (22) is also represented as

$$\beta_\mu \geq -c_3 \beta_m + c_4 \quad (63)$$

where $c_3 := [W_{m,u} \gamma_{m,u} + \zeta W_m \gamma_m] / [(1 + \zeta) W_\mu \gamma_\mu]$ and $c_4 := (1 + \zeta^{-1})^{-1} \left(1 + \frac{W_m \gamma_m}{W_\mu \gamma_\mu}\right)$.

The given P1 in Section IV-B is then equivalent to a the following graphical problem on the β_m - β_μ plane: maximizing the β_μ -intercept of (62) within the feasible region formed by (23) and (63). Solving this problem requires to consider the four possible cases for different settings in (63) as visualized in Fig. 10-a.

The cases 1 and 2 have the identical solution $(\beta_m^*, \beta_\mu^*) = \left(0, \left[1 + \frac{W_m \gamma_m}{W_\mu \gamma_\mu}\right] [1 + \zeta^{-1}]^{-1}\right)$, and share the same condition $\zeta \leq W_\mu \gamma_\mu / (W_m \gamma_m)$. Similarly, the cases 3 and 4 having the identical solution $(\beta_m^*, \beta_\mu^*) = \left(\left[\zeta - \frac{W_\mu \gamma_\mu}{W_m \gamma_m}\right] \left[\zeta + \frac{W_{m,u} \gamma_{m,u}}{W_m \gamma_m}\right]^{-1}, 1\right)$ share the same condition $\zeta > \frac{W_\mu \gamma_\mu}{W_m \gamma_m}$. Applying Theorems 1 and 2 to these results conclude the proof. \blacksquare

D. Proof of Proposition 5 (Optimal mm- μ W UL Resource Allocations with mmW UL Decoupling)

Consider $W_{m,u} \gamma_{m,u} < W_m \gamma_m$ that always holds in the cases without mmW UL decoupling. If this holds, the solutions with mmW UL decoupling are identical to the results in Proposition 3. In addition, it is necessary to consider $W_{m,u} \gamma_{m,u} \geq W_m \gamma_m$ under the cases with mmW UL decoupling. This corresponds with the scenarios where the mmW UL receptive BS densification overcomes the mmW UL bandwidth limitation. For such scenarios, the possible cases A and B are visualized in Fig. 10-b. These cases have the identical solution $(\beta_m^*, \beta_\mu^*) = \left(\left[1 + \frac{W_\mu \gamma_\mu}{W_m \gamma_m}\right] \left[1 + \frac{W_{m,u} \gamma_{m,u}}{\zeta W_m \gamma_m}\right]^{-1}, 0\right)$, and share the same condition $\zeta \leq W_{m,u} \gamma_{m,u} / (W_\mu \gamma_\mu)$. Note that this condition is always true due to the assumptions A1 and A2 in Section IV-B, and the opposite condition is thus false. Combining the solutions with Theorems 1 and 2 leads to the desired result. \blacksquare

ACKNOWLEDGEMENT

The authors are grateful to June Hwang and Minho Kim in Samsung Electronics for helpful feedback on the mmW overlaid cellular network architecture.

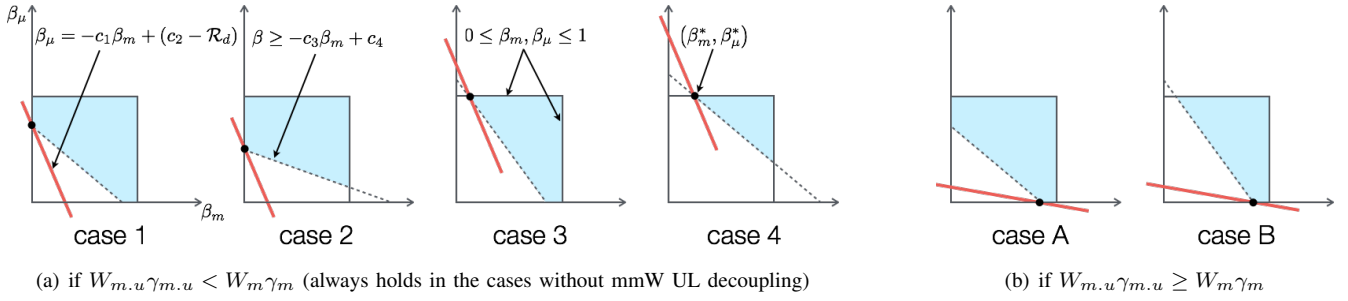


Fig. 10. Illustrations of the problem P1 in Section IV-B for different settings in (63) without and with mmW UL decoupling.

REFERENCES

- [1] Z. Pi and F. Khan, "An Introduction to Millimeter-Wave Mobile Broadband Systems," *IEEE Communications Magazine*, vol. 49, no. 6, pp. 101–107, 2011.
- [2] Z. Pi and F. Khan, "System Design and Network Architecture for a Millimeter-wave Mobile Broadband (MMB) System," in *Proc. IEEE Sarnoff Symposium, Princeton, NJ, United States*, 2011.
- [3] T. Kim, J. Park, J.-Y. Seol, S. Jeong, J. Cho, and W. Roh, "Tens of Gbps Support with mmWave Beamforming Systems for Next Generation Communications," *Proc. IEEE Global Communications Conference (GLOBECOM 2014)*, pp. 3685–3690, 2013.
- [4] Ericsson, "5G Radio Access," *Ericsson Review*, February 2015.
- [5] T. S. Rappaport, S. Sun, R. Mayzus, H. Zhao, Y. Azar, K. Wang, G. N. Wong, J. K. Schulz, M. Sammi, and F. Gutierrez, "Millimeter Wave Mobile Communications for 5G Cellular: It Will Work!," *IEEE Access*, vol. 1, pp. 335–349, 2013.
- [6] S. Ragan, T. S. Rappaport, and E. Erkip, "Millimeter-Wave Cellular Wireless Networks: Potentials and Challenges," *Proceedings of the IEEE*, vol. 102, no. 3, pp. 366–385, 2014.
- [7] J. G. Andrews, S. Buzzi, W. Choi, S. Hanly, A. Lozano, A. C. K. Soong, and J. C. Zhang, "What Will 5G Be?," *IEEE Journal on Selected Areas in Communications*, vol. PP, no. 99, 2014.
- [8] I. Hwang, B. Song, and S. S. Soliman, "A Holistic View on Hyper-Dense Heterogeneous and Small Cell Networks," *IEEE Communications Magazine*, vol. 51, no. 6, pp. 20–27, 2013.
- [9] J. Zander and P. Mähönen, "Riding the Data Tsunami in the Cloud: Myths and Challenges in Future Wireless Access," *IEEE Communications Magazine*, vol. 51, no. 3, pp. 145–151, 2013.
- [10] Qualcomm, "Hyper-Dense Small Cell Deployment Trial in NASCAR Environment," April 2014.
- [11] R. Baldmair, T. Irnich, K. Balachandran, E. Dahlman, G. Mildh, Y. Selén, S. Parkvall, M. Meyer, and A. Osseiran, "Ultra-Dense Networks in Millimeter-Wave Frequencies," *IEEE Communications Magazine*, vol. 53, no. 1, pp. 202–208, 2015.
- [12] T. Bai, R. Vaze, and R. W. Heath, Jr., "Analysis of Blockage Effects on Urban Cellular Networks," *IEEE Transactions on Wireless Communications*, vol. 13, no. 9, pp. 5070–5083, 2014.
- [13] T. Bai and R. W. Heath, Jr., "Coverage and Rate Analysis for Millimeter Wave Cellular Networks," available at: <http://arxiv.org/abs/1402.6430>.
- [14] S. M. Yu and S.-L. Kim, "Downlink Capacity and Base Station Density in Cellular Networks," *Proc. IEEE WiOpt Workshop on Spatial Stochastic Models for Wireless Networks (SpaWiN 2013)*, May 2013.
- [15] S. Lee and K. Huang, "Coverage and Economy of Cellular Networks with Many Base Stations," *IEEE Communications Letters*, vol. 16, no. 7, pp. 1038–1040, 2012.
- [16] A. G. Gotsis and A. Alexiou, "On Coordinating Ultra-Dense Wireless Access Networks: Optimization Modeling, Algorithms and Insights," available at: <http://arxiv.org/pdf/1312.1577v1.pdf>.
- [17] J. Park, S.-L. Kim, and J. Zander, "Asymptotic Behavior of Ultra-Dense Cellular Networks and Its Economic Impact," in *Proc. IEEE Global Communications Conference (GLOBECOM)*, Austin, TX, United States, December 2014.
- [18] J. Park, S.-L. Kim, and J. Zander, "Resource Management and Cell Planning in Millimeter-Wave Overlaid Ultra-Dense Cellular Networks," available at: <http://arxiv.org/abs/1504.05025>.
- [19] J. Park, S.-L. Kim, and J. Zander, "Tractable Resource Management in Millimeter-Wave Overlaid Ultra-Dense Cellular Networks," available at: <http://arxiv.org/abs/1507.04658>.
- [20] D. López-Pérez, M. Ding, H. Claussen, and A. H. Jafari, "Towards 1 Gbps/UE in Cellular Systems – Understanding Ultra-Dense Small Cell Deployments," available at: <http://arxiv.org/abs/1503.03912>.
- [21] C. Hoymann, D. Larsson, H. Koorapaty, and J.-F. Cheng, "A Lean Carrier for LTE," *IEEE Communications Magazine*, vol. 51, no. 2, pp. 74–80, 2013.
- [22] M. Thurfjell, M. Ericson, and P. d. Bruin, "Network Densification Impact on System Capacity," in *Proc. IEEE Vehicular Technology Conference (VTC), Spring, Glasgow, Scotland*, 2015.
- [23] C. Galiotto, N. K. Pratas, L. Doyle, and N. Marchetti, "Effect of LOS/NLOS Propagation on Ultra-Dense Networks," available at: <http://arxiv.org/abs/1507.01757>.
- [24] M. Ding, D. López-Pérez, G. Mao, P. Wang, and Z. Lin, "Will the Area Spectral Efficiency Monotonically Grow as Small Cells Go Dense?," available at: <http://arxiv.org/abs/1505.01920>.
- [25] X. Zhang and J. G. Andrews, "Downlink Cellular Network Analysis with Multi-slope Path Loss Models," available at: <http://arxiv.org/abs/1408.0549>.
- [26] D. Stoyan, K. W. S., and J. Mecke, *Stochastic Geometry and its Applications*. Wiley, 2nd ed., 1995.
- [27] D. Astely, E. Dahlman, G. Fodor, S. Parkvall, and J. Sachs, "LTE Release 12 and Beyond," *IEEE Communications Magazine*, vol. 51, no. 7, pp. 154–160, 2013.
- [28] S. Singh, M. N. Kulkarni, A. Ghosh, and J. G. Andrews, "Tractable Model for Rate in Self-Backhauled Millimeter Wave Cellular Networks," available at: <http://arxiv.org/abs/1407.5537>.
- [29] M. N. Kulkarni, S. Singh, and J. G. Andrews, "Coverage and Rate Trends in Dense Urban mmWave Cellular Networks," in *Proc. IEEE Global Communications Conference (GLOBECOM)*, Austin, TX, United States, December 2014.
- [30] J. Lee and C. Tepedelenlioglu, "Stochastic Ordering of Interference in Large-Scale Wireless Networks," *IEEE Transactions on Signal Processing*, vol. 62, no. 3, pp. 729–740, 2014.
- [31] B. Le, T. W. Rondeau, J. H. Reed, and C. W. Bostian, "Analog-to-Digital Converters," *IEEE Signal Processing Magazine*, vol. 22, no. 6, pp. 69–77, 2005.
- [32] J. G. Andrews, F. Baccelli, and R. K. Ganti, "A Tractable Approach to Coverage and Rate in Cellular Networks," *IEEE Transactions on Communications*, vol. 59, no. 11, pp. 3122–3134, 2011.
- [33] T. Jiang and Y. Wu, "An Overview: Peak-to-Average Power Ratio Reduction Techniques for OFDM Signals," *IEEE Transactions on Broadcasting*, vol. 54, no. 2, pp. 257–268, 2008.
- [34] H. Elshaer, F. Boccardi, M. Dohler, and R. Irmer, "Downlink and Uplink Decoupling: a Disruptive Architectural Design for 5G Networks," in *Proc. IEEE Global Communications Conference (GLOBECOM)*, Austin, TX, United States, 2014.
- [35] QGIS, available at: <http://www.qgis.org>.
- [36] 3GPP TS 36.306, Evolved Universal Terrestrial Radio Access (E-UTRA) User Equipment (UE) Radio Access Capabilities.
- [37] J.-S. Ferenc and Z. Nédá, "On the size-distribution of poisson voronoi cells," *Physica A: Statistical Mechanics and Its Applications*, vol. 35, no. 2, pp. 518–526, 2007.
- [38] M. Haenggi, *Stochastic Geometry for Wireless Networks*. Cambridge University Press, 2013.
- [39] M. Abramowitz and I. Stegun, *Handbook of Mathematical Functions*. Dover, 1972.